[redacted]

Development Report

R/S 3410 1327
THIS PUBLICATION CONTAINS
76 ~~0078~~ PAGES. COPY NO. 82
CF 0082 COPIES, SÉRIES A
TO 3428-2 FOR 3428-2

1st Review Date 3/09/98	Classification (Circle Numbers):
Authority: ☐ ADC ☒ ADD	1. Classification Retained
Name W Layne	2. Classification Changed to: U
2nd Review Date 3/17/98	3. Contains No DOE Classified Information
Authority:	4. Coordinate With:
Name R.B. Craner	5. Contains UCNI: NR
	6. Comments: OK for Opened

UNCLASSIFIED

RECORD COPY
Do Not Take From This Room

RS 3410/1327
SC-DR-68-594
February 1969

A ROLL CONTROL SYSTEM FOR SMALL REENTRY VEHICLE STABILITY AUGMENTATION (U)

SANDIA SYSTEMATIC DECLASSIFICATION REVIEW DOWNGRADING OR DECLASSIFICATION STAMP	
CLASSIFICATION CHANGED TO: U	AUTHORITY: R.B. Craner
Emilda Selph 4/30/98	
PERSON CHANGING MARKING & DATE	RECORD ID: 98SN1675
W. C. Layne 5/18/98	
PERSON VERIFYING MARKING & DATE	DATED: 3/17/98

A. F. Veneruso, 1223
Sandia Laboratories, Albuquerque

Back cover

[redacted]

Counted in

Pg Count

~~ATOMIC WEAPON DATA~~

~~STORMA 3~~

UNCLASSIFIED

SANDIA LABORATORIES

OPERATED FOR THE UNITED STATES ATOMIC ENERGY COMMISSION BY SANDIA CORPORATION | ALBUQUERQUE, NEW MEXICO, LIVERMORE, CALIFORNIA

[redacted]

[redacted] UNCLASSIFIED

SC-DR-68-594

A ROLL CONTROL SYSTEM FOR SMALL REENTRY VEHICLE STABILITY AUGMENTATION (U)

~~Atomic Weapon Data, Sigma 3~~

RS 3410/1327

A. F. Veneruso, 1223
Sandia Laboratories, Albuquerque

February 1969

Approved by: O. M. Stuetzer, 1220

ABSTRACT (U)

A mathematical model of reentry vehicle dynamics is used to analyze the requirements of a roll control system. A roll control system is then proposed, and the analytical tools required to perform the actual design are developed. These tools are developed independent of the particular types of components (fluidic, hydraulic, or electromechanical) used to realize the design.

[redacted]

[redacted]

[redacted]

UNCLASSIFIED

[redacted]

ACKNOWLEDGMENT

The advice and assistance of H. R. Vaughn, 9341, in formulating the aerodynamic techniques and models used through this study are acknowledged. In addition, the assistance of F. V. Wyatt, 9422, in developing and executing the analog computer programs for simulating the RV and control dynamics is acknowledged. The assistance of R. H. Braasch, 1223, in formulating the basic problem and verifying the resultant study is acknowledged.

SUMMARY

The peak torque and minimum total impulse requirements of a thruster roll control system for a reentry vehicle (RV) have been analyzed and found to be functions of the center-of-gravity offset and out-of-plane trim angle. The problem of control system-RV stability has also been analyzed. It was found that, if the control system thrust, delay time, and lag time constants are too large, undesirable control system behavior will result. Boundary conditions were developed for predicting the existence of such instability.

The sensing, switch, and output design characteristics of the proposed roll control system may be determined with the aid of the analytical tools developed in this report. These characteristics have been treated parametrically. Therefore this systems analysis is applicable in the general case, i.e., for realization of a control system by many types of components such as fluidic, electronic, or electromechanical for sensing and switching and monopropellant hydrazine or cold gas for thrusters.

It must be emphasized that the aerodynamic models and simulations used in this study are exceedingly simple when compared to the real situation. The intention of this study, however, is to provide a foundation for efforts in component development, advanced aerodynamic and control system analysis and simulation, and vehicle damage assessment studies.

Our analysis approach has been based upon development of a simulation capability with the following order of refinement:

1. Linear Analog Computation
2. Nonlinear Analog Computation
3. Digital Computation
4. Hybrid Computation

The present status finds us available to perform analysis via the first three categories defined above.

TABLE OF CONTENTS

	Page
SUMMARY	5
Introduction	15
Aerodynamic Model	16
Theory	16
Application	20
Roll Control System	30
Roll Torque Requirements	30
Total Impulse Requirements	31
Basic Control System	35
Switching Function Analysis	36
Switching Function Hysteresis	37
Switching Function Dead Time	39
Thruster Characteristics	40
Limit Cycle Behavior with Thruster Lag and Zero Dead Time	42
System Phase Plane Portrait	43
Undesirable Limit Cycles	46
Limit Cycle Behavior with Thruster Lag and Nonzero Dead Time	50
Design Examples	51
Analog Simulation of Roll Control Systems	56
Comparison Between Digital and Analog Computer Simulations	63
Desiderata	66
Stability Before and After X-Ray Exposure	66
Magnitude of Aerodynamic Roll Torque	68
Effects of In-Plane Trim Angle	68
Sizing and Component Analysis for Roll Control	68
Tradeoff Study of Active and Passive Roll Control	69
Compensation and Adaptation Study	70
LIST OF REFERENCES	71

LIST OF ILLUSTRATIONS

Figure		Page
1a	Axes System with Generalized Asymmetry	17
1b	Axes System Showing Positive Out-of-Plane Trim Angle	17
2	Diagram of Asymmetry Moments	18
3	Dynamic Pressure Versus Time	21
4	Magnitude of Velocity Versus Time from 300,000 Feet	21
5	Analog Simulation of RV Dynamics Showing Spinup	23
6	Analog Simulation of RV Dynamics Showing Spinup	24
7	Analog Simulation Showing Spinup and Transient Effects	25
8	Analog Simulation Showing Spinup and Transient Effects	26
9	Analog Simulation Showing Resonance Effects	27
10	Analog Simulation Showing Roll Reversal	28
11	Analog Simulation Showing Roll Reversal	29
12	Dynamic Pressure Versus Time	33
13	Basic Bang-Bang-Off Roll Control System	35
14	Thruster Nozzle Geometry	36
15a	Switching Function Output	38
15b	Switching Function Output with Hysteresis	38

LIST OF ILLUSTRATIONS (cont)

Figure		Page
16	Thruster Input-Output Characteristics	41
17	Complete Roll Control System Model	42
18	Phase Plane Portrait ($q' = 60,000$ lb/ft^2)	44
19	Phase Plane Portrait ($q' = 20,000$ lb/ft^2)	45
20	Analog Generated Phase Plane Portrait	47
21	Undesirable Limit Cycle	48
22	Analog Simulation with Roll Control (Small Asymmetries)	58
23	Analog Simulation with Roll Control (Nominal Asymmetries)	59
24	Analog Simulation with Roll Control (Large Asymmetries)	60
25	Analog Simulation with Roll Control (Large Asymmetries) Higher Control Thrust	61
26	Analog Simulation with Roll Control (Small Asymmetries)	62
27	Analog Simulation with Roll Control (Undesirable Limit Cycle)	64
28	Comparison Between Digital and Analog Simulations	65
29	Digital Simulation with Roll Control	67

LIST OF SYMBOLS

a	Exponential constant for dynamic pressure approximation, $1/\text{sec}^2$
C_{Mq}	Coefficient of pitch damping moment, $\frac{\partial}{\partial \frac{\dot{\theta}\ell}{2V}} \left(\frac{\text{damping moment}}{q's\ \ell}\right), \frac{1}{\text{rad}}$
$C_{M\theta}$	Coefficient of rate of change of pitching moment with total angle of attack, $\frac{\partial}{\partial\theta} \left(\frac{\text{pitching moment}}{q's\ \ell}\right), \frac{1}{\text{rad}}$
$C_{N\theta}$	Coefficient of normal force due to total angle of attack, $\frac{\partial}{\partial\theta} \left(\frac{\text{normal force}}{q's}\right), \frac{1}{\text{rad}}$
d	Base diameter, ft
F	Instantaneous value of thrust from each jet thruster, lb
F_c	Instantaneous value of thrust at time T_c when $p = p_c$, sec
F_0	Steady state or final value thrust from each jet thruster, lb
h	Altitude, ft
I	Moment of inertia about any transverse axis for rotationally symmetrical body, $I = I_y = I_z$, slug ft^2
$\mathcal{I}$	Total impulse, lb sec
$\mathcal{I}_{sim}$	Total impulse required during simulation, lb sec
I_x	Moment of inertia about x axis, slug ft^2
I_y	Moment of inertia about y axis, slug ft^2
I_z	Moment of inertia about z axis, slug ft^2

LIST OF SYMBOLS (cont)

L_{ax}	Roll moment due to asymmetries, ft-lb
$L_{ax_{DC}}$	Short-term average or DC roll moment, ft-lb
$L_{ax_{peak}}$	Maximum roll moment, ft-lb
L_u	Roll moment due to control thrust, ft-lb
ℓ	Reference length, RV length, ft
M_q	Rate of change of damping moment with rate of change of total angle of attack, $\frac{\text{ft-lb}}{\text{rad/sec}}$
M_θ	Rate of change of pitching moment with total angle of attack in aeroballistic system, $\frac{\text{ft-lb}}{\text{rad}}$
N_θ	Normal force due to total angle of attack, lb/rad
p	Roll rate, angular velocity of body about x or $\bar{x}$ axis, rad/sec
p'	Constant used as an intermediate in evaluating boundary conditions
p_a, p_b, p_c, p_d	Switching points of roll rate sensing with sensor hysteresis, rad/sec
p_H, p_L	High and low values of roll rate sensing threshold, rad/sec
$p^+_{T_{sd}}$	Roll rate increase during sensor dead time, T_{sd}, rad/sec
$p^-_{T_{sd}}$	Roll rate decrease during sensor dead time with roll down thruster on, rad/sec
q'	Dynamic pressure, $1/2\rho V^2$, lb/ft^2
q'_m	Peak dynamic pressure, lb/ft^2
r_m	Moment arm from RV centerline to a thruster, ft

LIST OF SYMBOLS (cont)

S	Base area, $\frac{d^2}{4}$, ft^2
s	Laplace transform variable
t	time, sec
T	Dummy time variable, sec
T^*	Time at which aerodynamic torque equals control torque, sec
T_{ad}	Roll rate sensor dead time, sec
T_c	Time at which $p = p_c$, sec
T_D	Total equivalent control system dead time, sec
T_f	Time limit for integrating dynamic pressure, sec
T_{sd}	Switching function dead time, sec
T_{Td}	Thruster dead time, sec
T_1, T_2	Time required for roll rate p to go from p_c to p_d and p_d back to p_c
T_{on}	Thruster on time pulse duration, sec
T_{off}	Thruster off time pulse duration, sec
u	Control switching variable, $u = -1, 0, +1$
V	Total free stream air velocity ft/sec
X	Inertial axis colinear with free-strem velocity (perpendicular to Y and Z axes)
x	Axis of roll
x'	Reference axis parallel to x axis and intersecting the aerodynamic axis in the x-y plane
x_{cp}	Static margin, distance along x_s axis from CG to aerodynamic center of pressure (negative for static stability), ft
x_s	Axis of aerodynamic symmetry
Y	Inertial axis perpendicular to X and Z
y	Body fixed pitch axis perpendicular to x and y axis

LIST OF SYMBOLS (cont)

y_0	Distance (CG offset) from center of gravity to axis of aerodynamic asymmetry, ft
Z	Inertial reference axis perpendicular to X and Y axes
z	Body fixed yaw axis perpendicular to x and y axes
α	Angle of attack about y axis, rad
α_t	Out-of-plane trim angle, rad
γ	Flight path angle measured between local horizontal and flight path, deg
θ	Total angle of attack, angle between X and x axis, rad
ψ	Total yaw or precession angle, angle between Y axis and θ plane and in Y-Z plane, rad
ϕ	Roll angle, angle between θ plane and y axis in y-z plane, rad
η	Time variable for approximate dynamic pressure, $\eta = t-33.0$, sec
τ	Thruster lag time constant, sec
ξ	Constant used as an intermediate in evaluating boundary conditions

A ROLL CONTROL SYSTEM FOR SMALL REENTRY VEHICLE STABILITY AUGMENTATION

Introduction

In computer simulations and actual flight tests, small reentry vehicles (RV) have exhibited dynamic instabilities such as roll reversal, spin-up, and roll resonance. These instabilities have resulted in either catastrophic vehicle failure or large dispersions on the order of thousands of feet from the intended target.[1] Analysis of these instabilities is the subject of aerodynamic research. In particular, many of the analytical techniques necessary to predict the onset of roll resonance and the magnitude change in roll rate due to vehicle asymmetries have been developed.[2,3,4]

It has been found that for a small RV, spin-up or roll reversal may be produced by very small asymmetries.[4,5] In fact, for an RV weighing less than 250 pounds, an out-of-plane trim angle of 0.1 degree or greater in combination with a center-of-gravity (CG) offset of 0.050 inch or greater will cause significant changes in the roll rate.[4] Even though the CG offset can be measured statically to ±0.020 inch,[6] this does not guarantee the roll rate because the CG offset and out-of-plane trim angle may change during reentry due to nonuniform ablation and heating or as a result of an interception by an antiballistic missile (ABM). Thus an RV may be designed to physically survive the effects of interception by an ABM at a given range only to be destroyed by aerodynamic instabilities during reentry.

These effects provide impetus to investigate schemes for stability control of reentry vehicles. Since spin-up, roll reversal, and roll resonance are caused by aerodynamic roll torques, a control system which provides an opposing torque about the roll axis would augment the stability of the RV. The type of control system required to augment RV stability will be investigated in the following paragraphs. First, however, the dynamics of the RV will be developed and parameters affecting the design of the roll control system will be identified and examined.

Aerodynamic Model

Theory

H. R. Vaughn[2, 3] has developed a 3-degree-of-freedom axis system that greatly simplifies the mathematical description of the RV dynamics in roll, pitch, and yaw. In this system, x, y, and z are body fixed areas; the position of these axes with respect to the inertial axis system, X, Y, and Z, is defined by the three angles ψ, θ, and ϕ. The origin of both sets of axes is at the vehicle center of gravity (CG). In general, the axis of aerodynamic symmetry, x_s, may not be colinear or parallel with the body principal axis x. Figure 1a displays the axes system and the general relation between the body principal axis, x, and the aerodynamic axis, x_s. In Figure 1b, the axis system is shown with an out-of-plane trim angle, α_t, between the aerodynamic axis and the x-y plane. By definition, α_t is measured about the y axis. The center of gravity offset, y_0, is shown to be the distance from the CG to the aerodynamic axis and measured along the y axis. A reference vector, x', has been constructed in the x-y plane parallel to x and interesecting the aerodynamic axis at the CG offset. The center of pressure (CP) is on the aerodynamic axis and slightly behind the CG by a distance defined as the static margin, X_{CP}.

Figure 2 diagrams the asymmetry moments for small $\alpha_t > 0$. The normal lift produced by the angle of attack contributes a force $N_\theta \theta \cos \theta$ at a moment arm $y_0 \sin \phi + X_{CP} \sin \alpha_t \cos \phi$ or $y_0 \sin \phi$ since $\sin \alpha_t \cong 0$. The out-of-plane trim angle contributes a force $N_\theta \alpha_t \cos \alpha_t$ at a moment arm y_0. Since α_t and θ are assumed small, $\cos \alpha_t \cong 1$ and $\cos \theta \cong 1$.

By summing the moments about the x axis and discarding negligible terms, the roll moment equation may be developed:[2]

$$\dot{p} I_x = N_\theta \theta y_0 \sin \phi + N_\theta \alpha_t y_0 = 0 \quad . \tag{1}$$

The terms in the above equation may be visualized with the aid of Figure 2b. The first term is simply the inertial moment, the second is the primary "roll lock-in" moment, and the third term contributes to both lock-in, spin-up, and roll reversal by providing a roll torque due to α_t with moment arm y_0.

UNCLASSIFIED

[redacted]

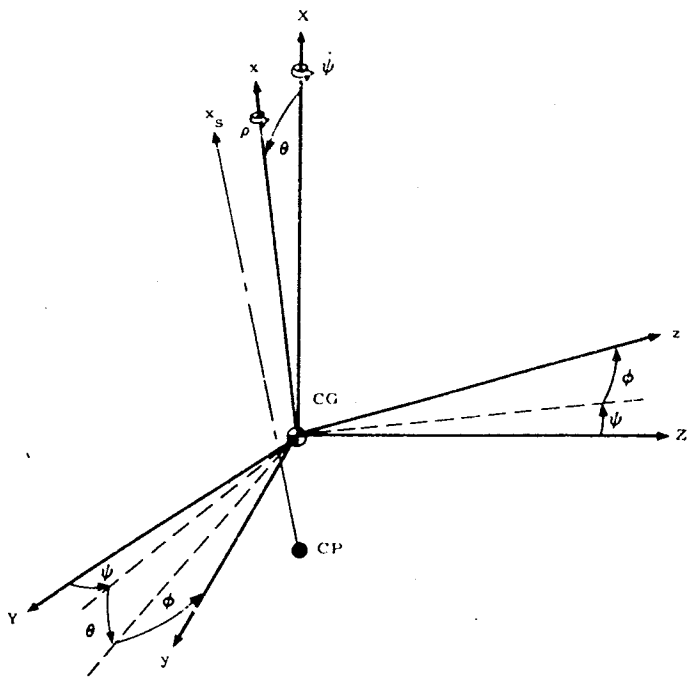

Figure 1a. Axes System with Generalized Asymmetry

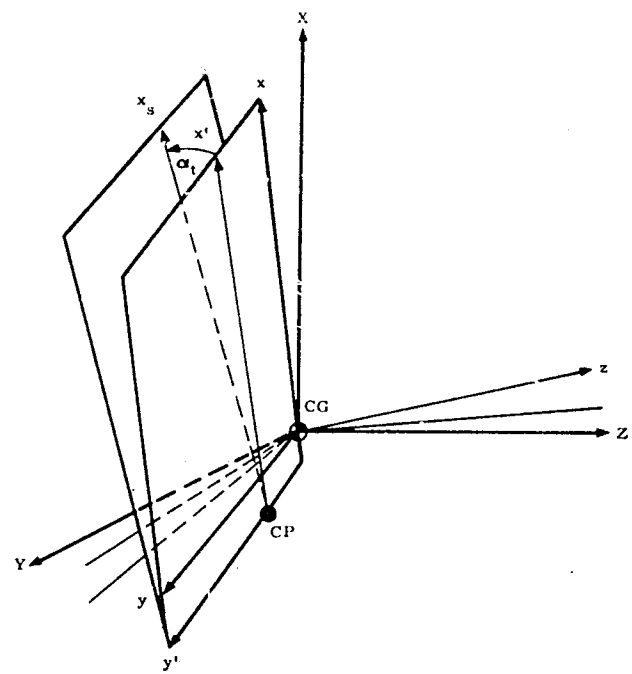

Figure 1b. Axes System Showing Positive Out-of-Plane Trim Angle

[redacted]

UNCLASSIFIED

Moment arm for $N_\theta \theta \cos \theta$

$$y_0 \sin \phi + x_{cp} \sin \alpha_t \cos \phi$$

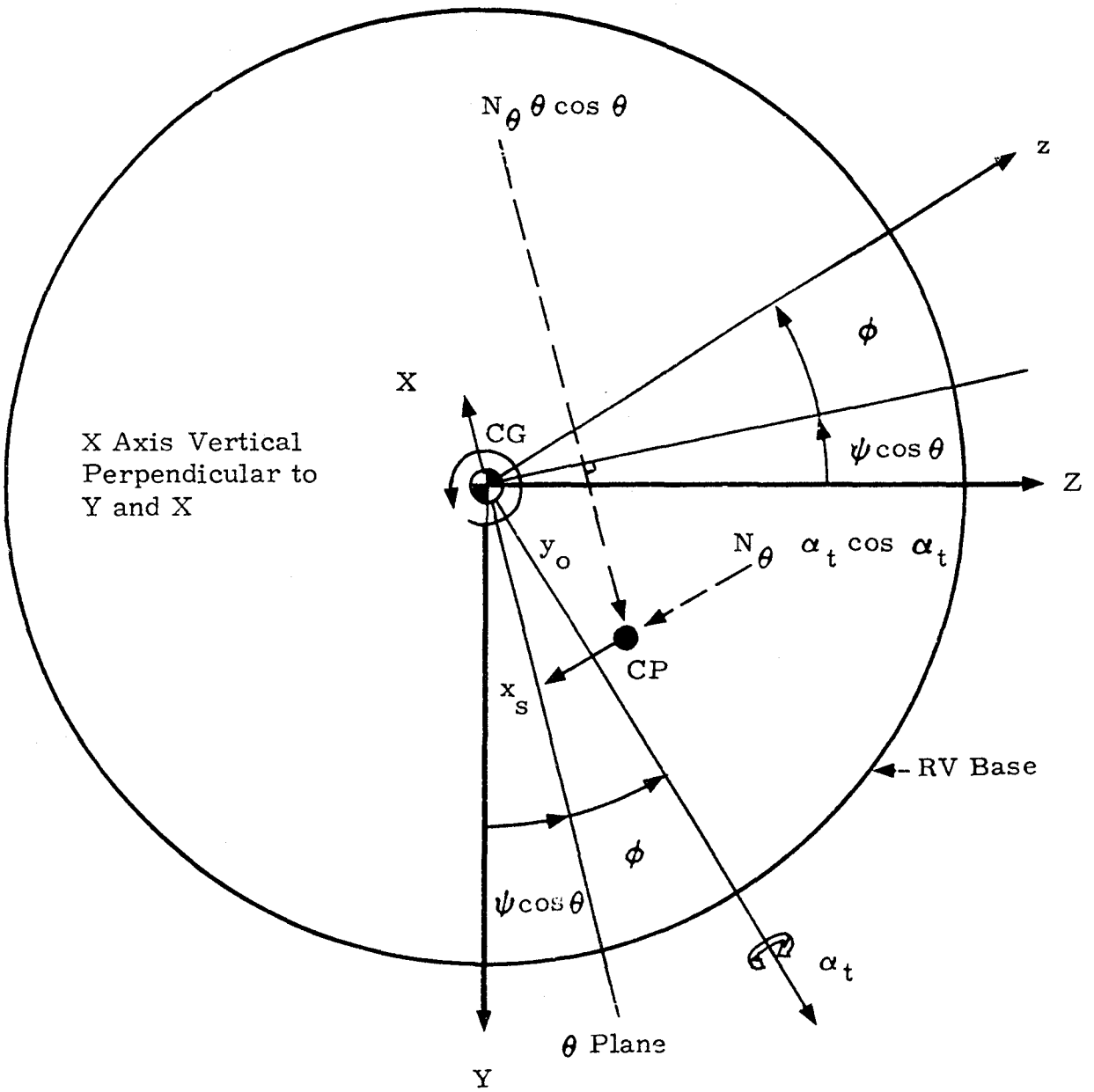

Figure 2. Diagram of Asymmetry Moments

If a roll control system is added to the vehicle, Equation 1 should be modified to incorporate a control torque $L_u u$:

$$pI_x + N_\theta \theta y_0 \sin \phi + N_\theta \alpha_t y_0 - L_u u = 0 \ . \tag{2}$$

The details of the control system for producing $L_u u$ will be investigated in the next section.

By inspecting Figure 1, the change in roll angle, ϕ, may be expressed as the roll rate, p, minus the projection of the change in yaw angle, ψ, on to the roll axis, x, or

$$\dot{\phi} = p - \dot{\psi} \cos \theta \ . \tag{3}$$

In order to describe the pitch dynamics, the moments about the Z-axis may be written[7]

$$M_y = I\ddot{\theta} - \overset{(-)}{M_q}\dot{\theta} - \overset{(-)}{M_\theta}\theta = 0 \ . \tag{4}$$

The negative sign placed above M_q and M_α is a reminder that for a stable vehicle these quantities are negative.

The out-of-plane trim angle, α_t, acts as a forcing function on the pitch dynamics since α_t rotates with the roll rate about x'. Since x' is parallel to the principle axis (x) of the RV, the aerodynamic lift due to α_t alternately adds to and subtracts from the pitch angle, θ.

When the effect of the out-of-plane trim angle is included in the pitch dynamics, the result is

$$I\ddot{\theta} - \overset{(-)}{M_q}\dot{\theta} - \overset{(-)}{M_\theta}\theta = -\overset{(-)}{M_\theta}\alpha_t \cos pt \ . \tag{5}$$

The three differential equations which describe the simplified aerodynamics are then:

$$\dot{p} = -\frac{N_\theta y_0}{I_x}(\theta \sin \phi + \alpha_t) + \frac{L_u u}{I_x} \ , \tag{6}$$

$$\dot{\phi} = p - \dot{\psi} \cos \theta \ , \tag{7}$$

$$\ddot{\theta} - \frac{\overset{(-)}{M_q}\dot{\theta}}{I} - \frac{\overset{(-)}{M_\theta}\theta}{I} = - \frac{\overset{(-)}{M_\theta}}{I} \alpha_t \cos pt \ . \tag{8}$$

The above equations may be written with aerodynamic coefficients $C_{N\theta}$, C_{Mq}, and $C_{M\theta}$, in that

$$N_\theta = C_{N\theta} S q' \ , \tag{9a}$$

$$M_q = \frac{C_{Mq} \ell^2 q' S}{2V} \ , \tag{9b}$$

and

$$M_\theta = C_{M\theta} S \ell q' \ . \tag{9c}$$

If $\ddot{\theta}$ and θ are small and for circular coning motion, the summation of moments about the y-axis may be used to obtain a simple approximation to $\dot{\psi}$.[2]

$$\dot{\psi} \approx \sqrt{- \frac{\overset{(-)}{M_\theta}}{I}} \ \text{rad} \ . \tag{10}$$

Application

An analog computer was used for this initial investigation since the nonlinearities and time-varying nature of the problem required that many different values of control system and vehicle parameters be studied in detail. Also the flexibility and ease with which the analog program may be changed enables the investigation of many different types of control systems.

Sandia Laboratories' analog computer facility was therefore programmed with Equations 6, 7, and 8 using the relations 9 and the approximation 10. The constant values were derived from one of the Castor designs and are given in Table I. The dynamic pressure, q', and the magnitude of the velocity vector, v, are programmed as functions of time and are shown in Figures 3 and 4. These functions were obtained from the output of a 6-degree-of-freedom (6DOF) digital computer simulation of the

UNCLASSIFIED

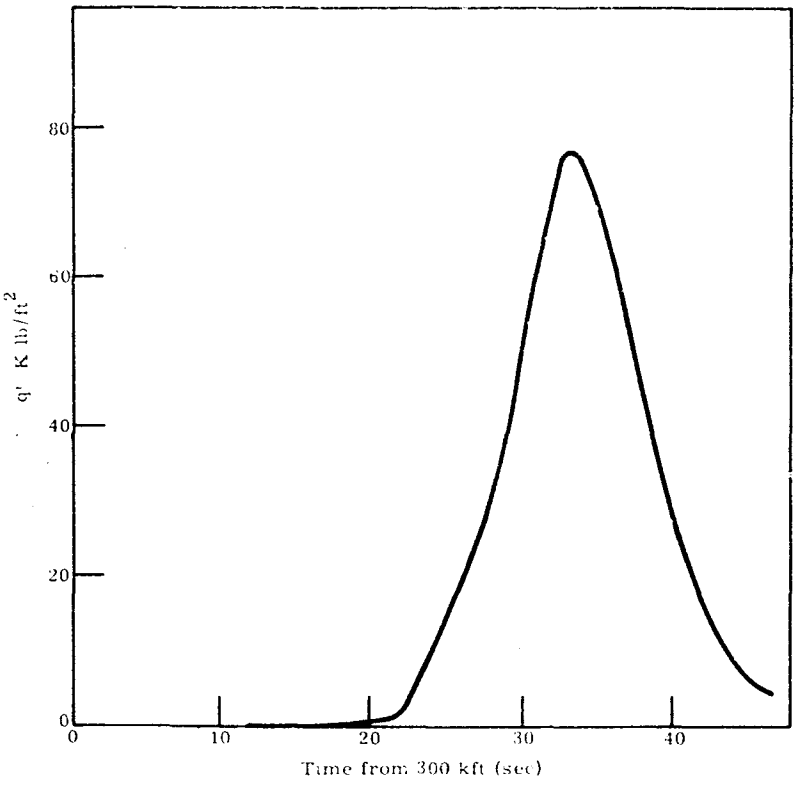

Figure 3. Dynamic Pressure Versus Time

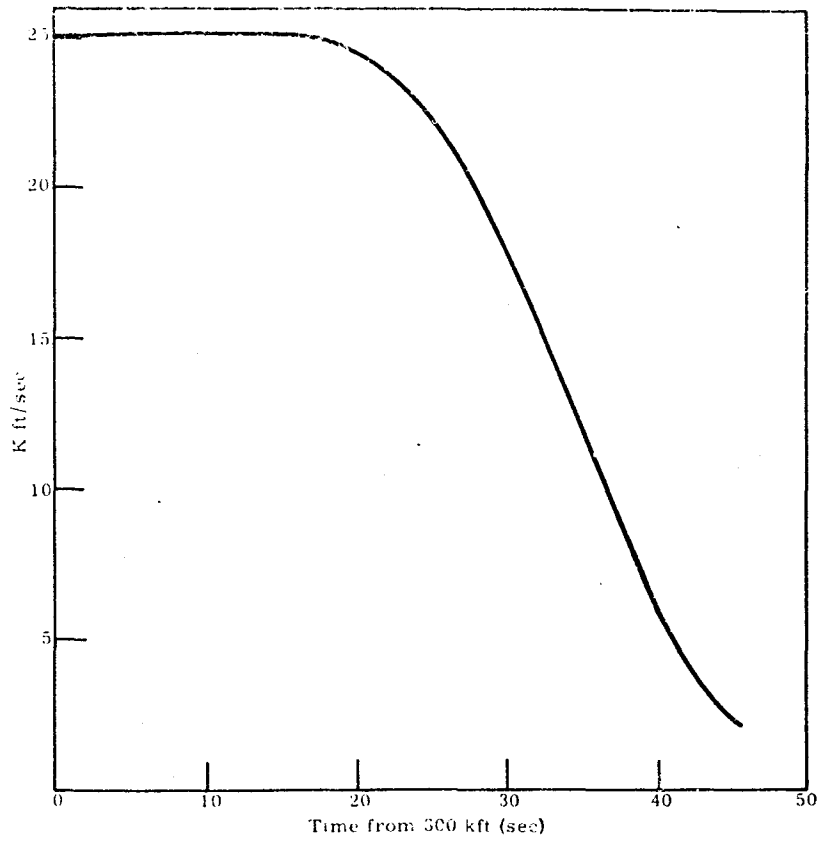

Figure 4. Magnitude of Velocity Versus Time from 300,000 Feet

UNCLASSIFIED

Castor reentry vehicle with a flight path angle of -20 degrees and an initial reentry velocity (at 300 kilofeet) of 25,000 fps.

TABLE I

Physical and Aerodynamic Constants from Castor Design Used in Analog Simulation

$S = 0.852 \text{ ft}^2$

$I = 3.61 \text{ slug ft}^2$

$I_x = 0.225 \text{ slug ft}^2$

$\ell = 4.58 \text{ ft}$

$C_{N\theta} = 1.433$ per radian

$C_{Mq} = -0.1347$ per radian

Since the 6DOF simulation was made with $y_0 = 0$, the resulting q' and v functions, used to program the analog computer, are valid only as long as the pitch and yaw angles are small and the absolute value of the roll rate is small enough so Equations 6 through 10 are a good approximation to the vehicle dynamics.

A comparison will be made in this report between results obtained with the 6DOF codes and the analog for several values of y_0 and α_t.

Figures 5 through 11 display the roll rate, p, the angle of attack, and the yaw rate, $\dot{\psi}$, as functions of time for various asymmetries. Stability analysis for the determination of suitable values of roll rate has been performed.[8] This analysis is based upon the sensitivity of the boundary conditions for persistent roll resonance[3] to dynamic pressure during reentry. For the simulations, the initial roll rate was 18.8 rad/sec.

Note that even with small asymmetries (0.025 inch and -0.5 degree, Figure 5), the roll rate may build up to high values (100 radians/second) where the centrifugal forces on the vehicle are large. For example, in Figure 5 where p = 100 radians/second, the centrifugal acceleration on a 6-inch moment arm is 155 g.

Notice the growth in angle of attack, θ, in Figures 7, 8, and 9 whenever the roll rate equals the yaw rate, $\dot{\psi}$. These large angles of attack would result in high drag forces on the vehicle which may exceed the structural load limits of the vehicle or result in large dispersions from the intended target. In Figure 9, the roll rate becomes locked-in for a short time during which the angle of attack reaches a maximum of 12.75 degrees.

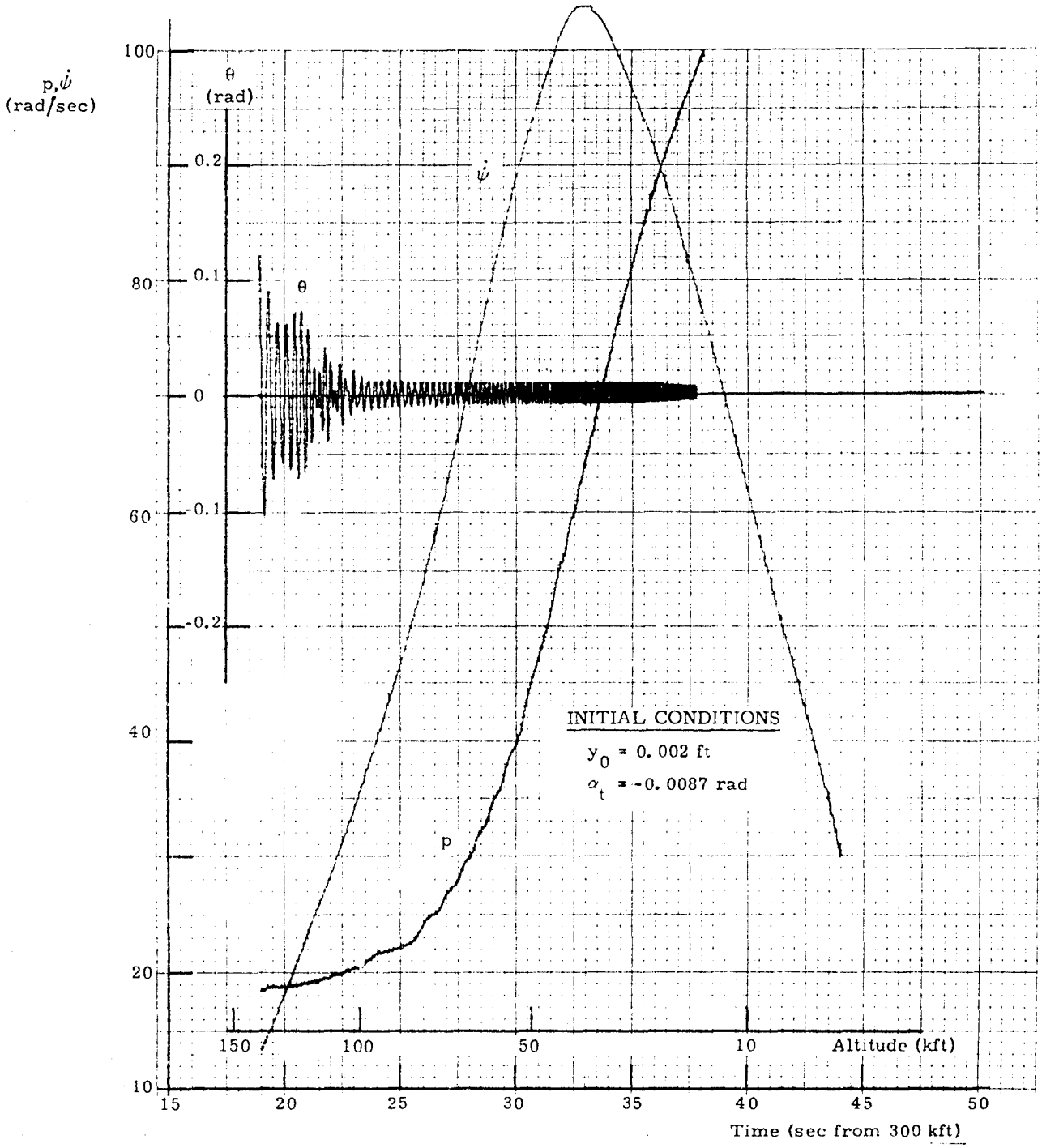

Figure 5. Analog Simulation of RV Dynamics Showing Spinup

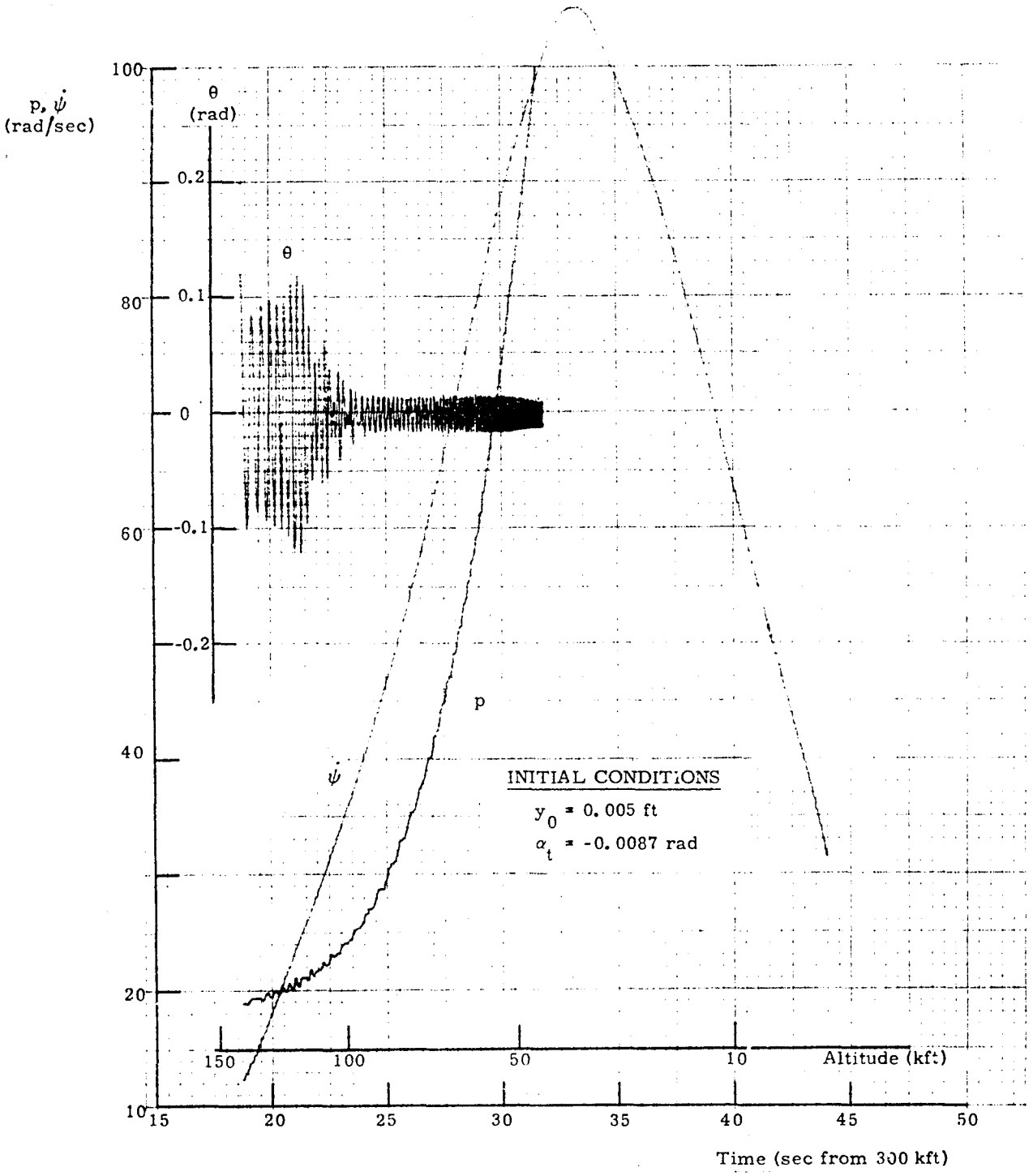

Figure 6. Analog Simulation of RV Dynamics Showing Spinup

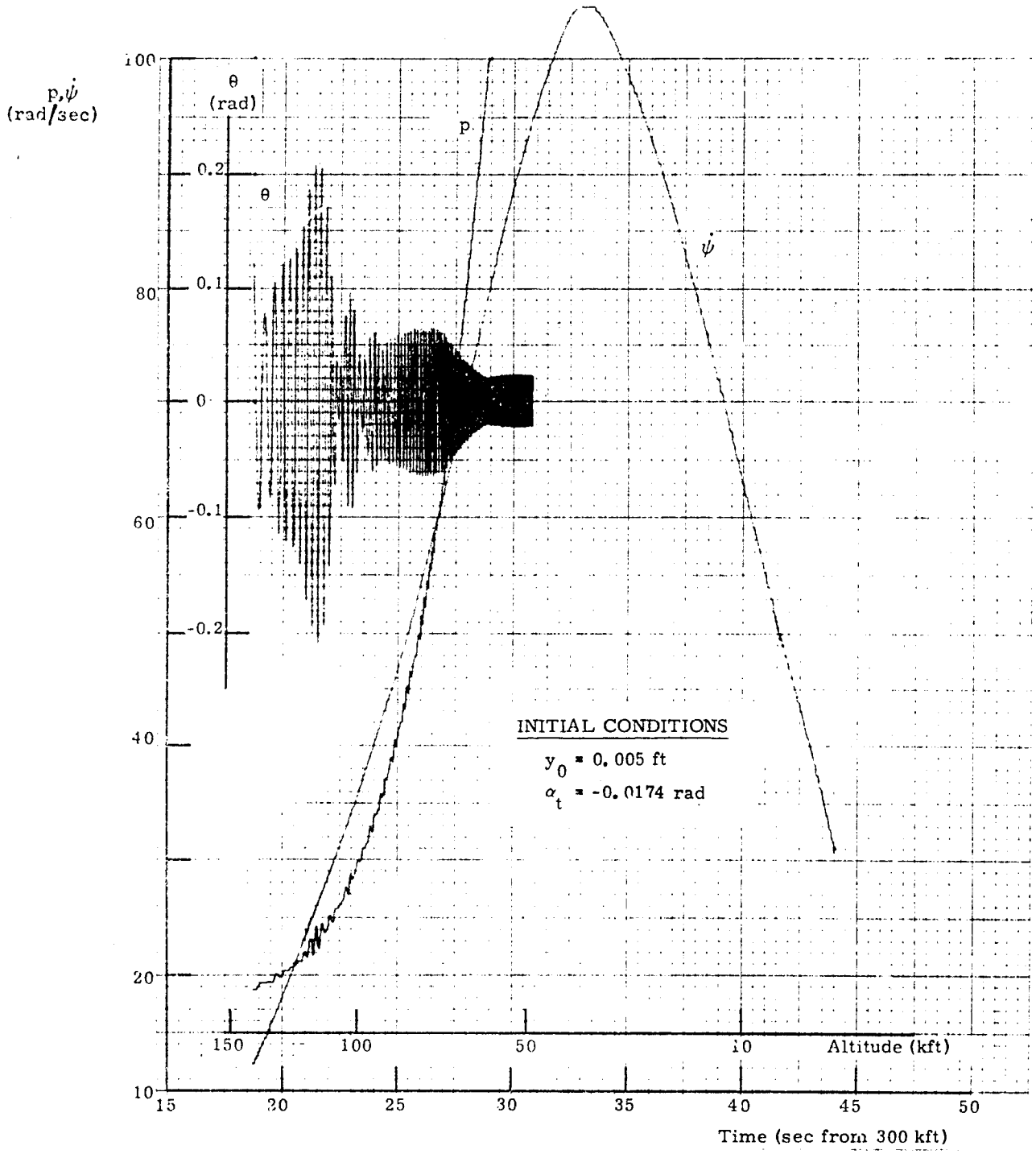

Figure 7. Analog Simulation Showing Spinup and Transient Effects

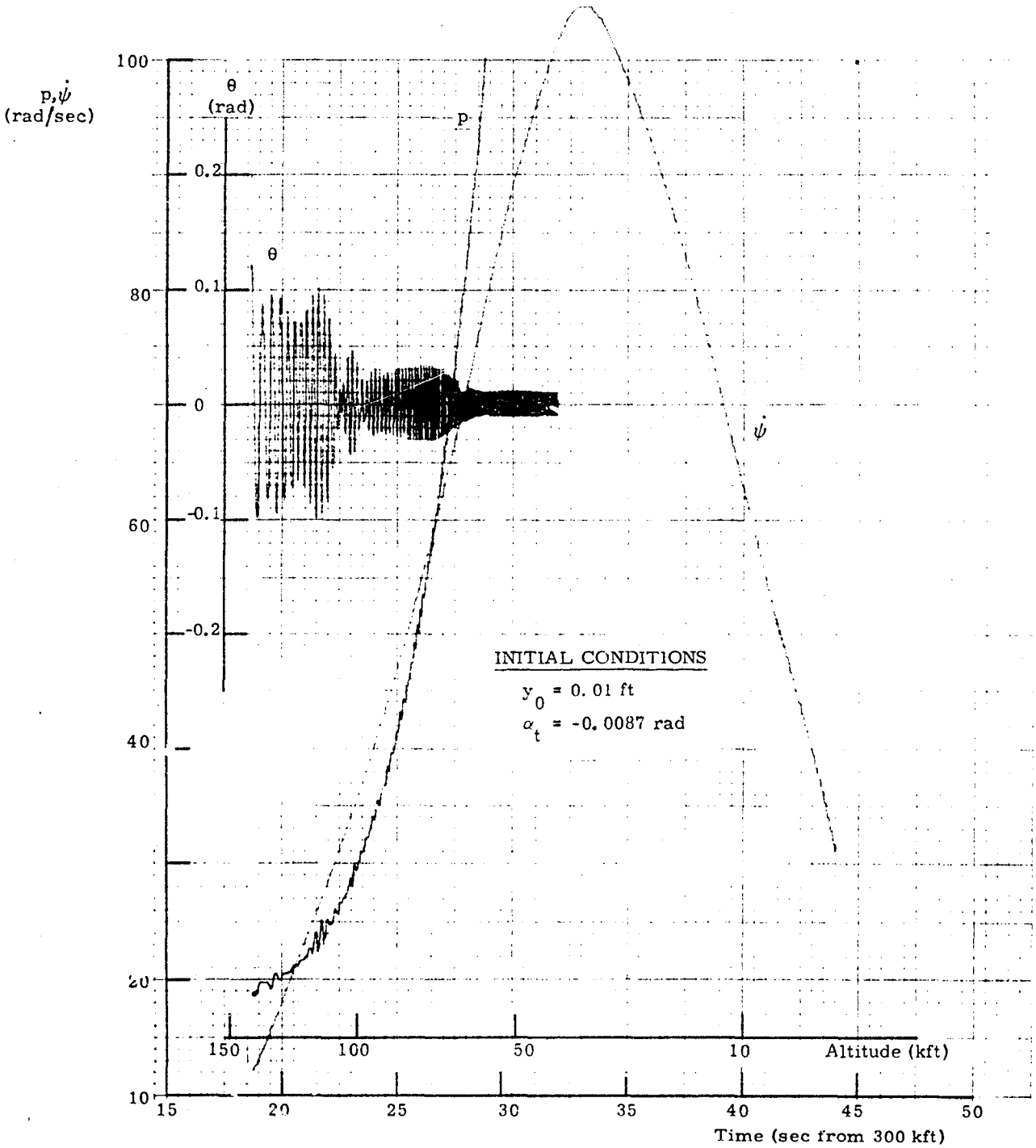

Figure 8. Analog Simulation Showing Spinup and Transient Effects

[redacted]

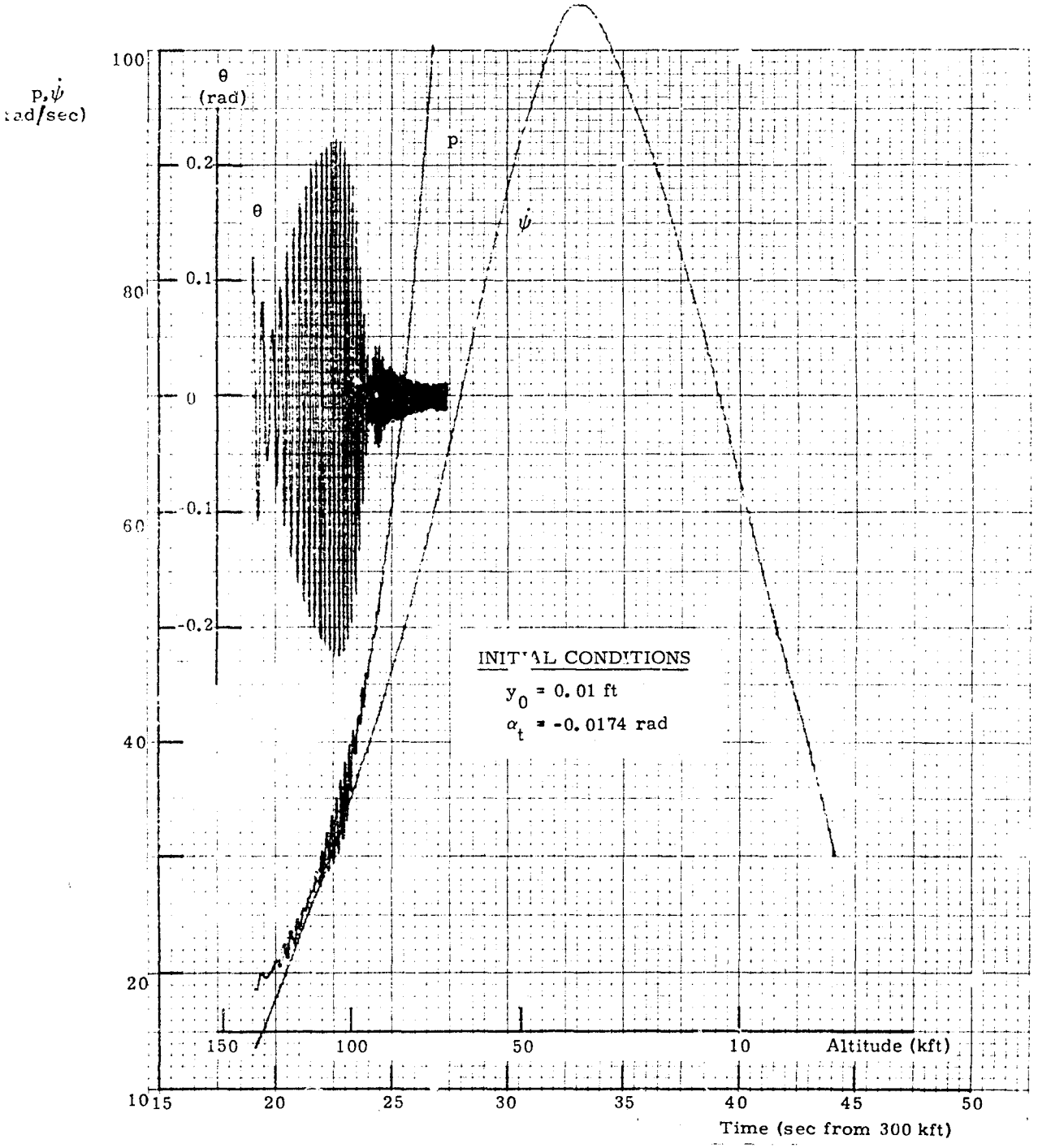

Figure 9. Analog Simulation Showing Resonance Effects

[redacted]

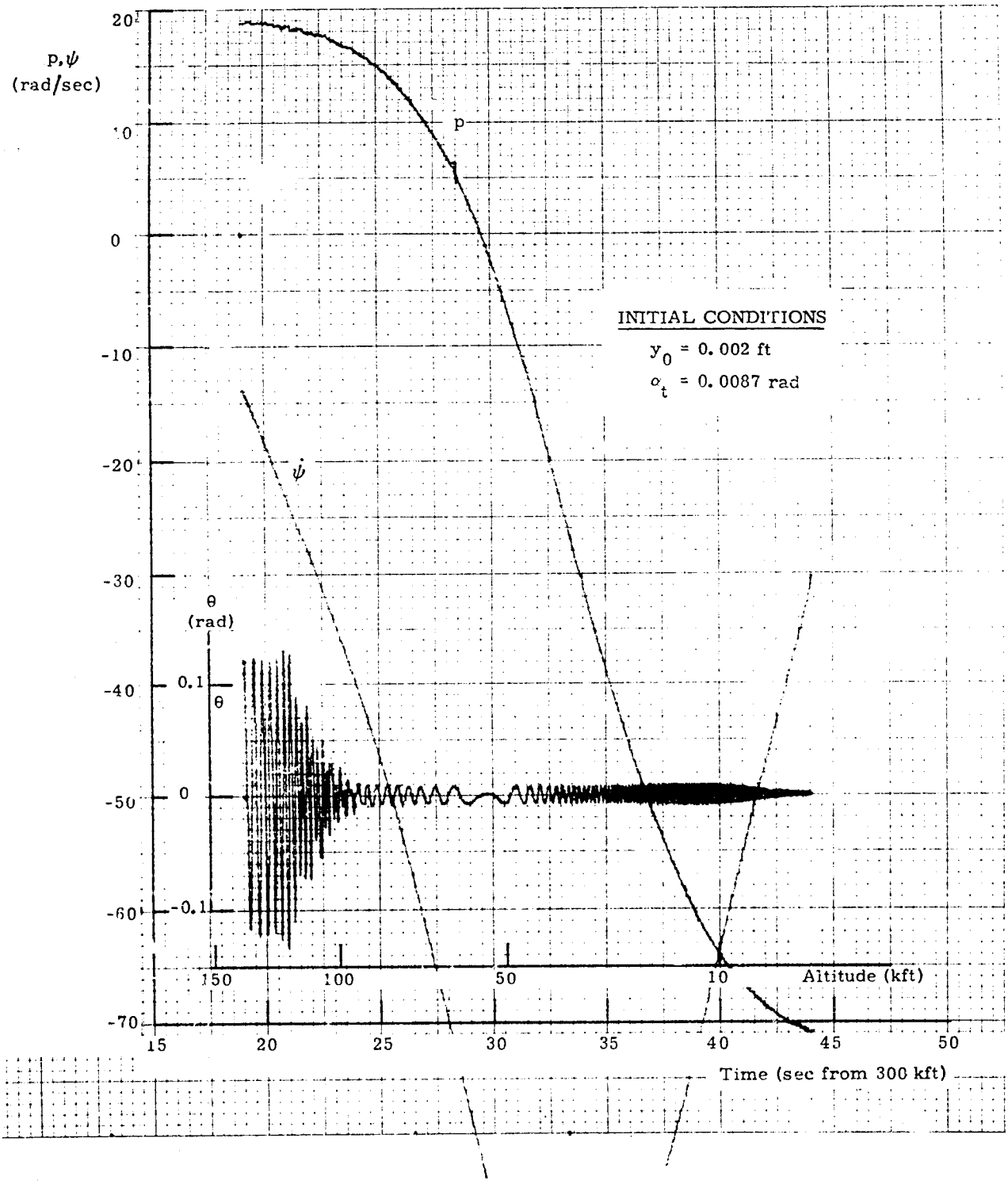

Figure 10. Analog Simulation Showing Roll Reversal

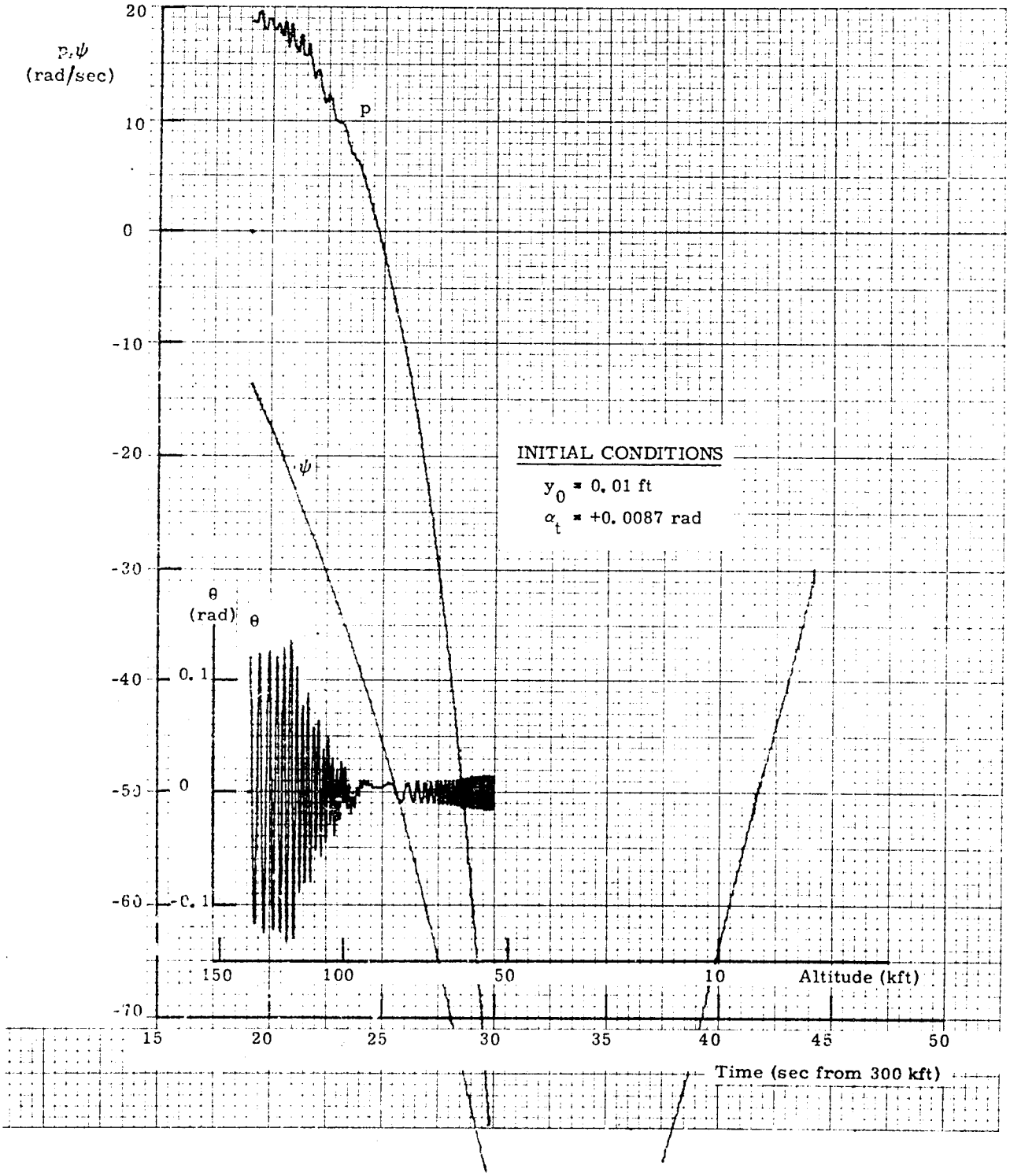

Figure 11. Analog Simulation Showing Roll Reversal

Figures 10 and 11 were obtained for out-of-plane trim angles with positive signs; the resulting motion is roll reversal. In roll reversal, the roll rate, p, goes through zero to negative values. In these two plots, the negative image of the yaw rate, $-\dot{\psi}$, is given since resonance can also occur if $p = -\dot{\psi}$.[2] This phenomenon is shown in Figure 11. The roll rate goes through zero and approaches $-\dot{\psi}$, and the angle of attack grows from 0.5 degree to 1.0 degree at t = 30 seconds from 300 kilofeet.

Roll Control System

Roll Torque Requirements

If the RV has a CG offset, y_0, and an out-of-plane trim angle, α_t, then a torque about the roll axis, x, is developed. It is this torque which the roll control system must counteract. The geometry of the forces producing this torque is shown in Figure 2. From Equation 1 this torque is

$$L_{ax} = -N_\theta y_0(\theta \sin \phi + \alpha_t) \text{ ft lb} . \tag{11}$$

If $p \neq \dot{\psi}$ is assumed, then Equation 3 shows that $\dot{\phi} \neq 0$ and therefore $\sin \phi$ is alternating sign at a frequency approximately equal to $p - \dot{\psi}$. Therefore, so long as $p \neq \dot{\psi}$, the short-term average or DC torque from Equation 11 is

$$L_{ax\,DC} = -N_\theta y_0 \alpha_t \text{ ft lb} . \tag{12}$$

When $p = \dot{\psi}$, and α_t is a negative number, the peak torque is achieved with $\phi = -\pi/2$, or

$$L_{ax\,peak} = N_\theta \Big|_{p=\dot{\psi}} y_0(\theta - \alpha_t) \text{ ft lb} . \tag{13}$$

Thus the peak torque required is a function of y_0, α_t, θ, and N_θ at the time when $p = \dot{\psi}$.

Total Impulse Requirements

By definition, the total impulse, I, is

$$\mathcal{I} = \int_0^{t_f} F(t)dt \text{ lb sec} , \tag{14}$$

where F(t) is the thrust versus time function and t_f is the time interval over which ℓ must be computed.

Since the control torque must counteract the aerodynamic roll torque, the thrust required is

$$F \geq \frac{N_\theta y_0 \alpha_t}{r_m} \text{ lb} , \tag{15}$$

where r_m is the moment arm from the principal axis of the vehicle to the thruster.

The total impulse must then be

$$\mathcal{I} \geq \int_0^{t_f} \frac{N_\theta y_0 \alpha_t}{r_m} dt . \tag{16}$$

Using relation 9a,

$$\mathcal{I} \geq \int_0^{t_f} \frac{C_{N\theta} S q' y_0 \alpha_t}{r_m} dt . \tag{17}$$

Since $C_{N\theta}$, S, y_0, α_t, and r are assumed to be constant with respect to time, Equation 17 may be rewritten:

$$\mathcal{I} \geq \frac{C_{N\theta} S y_0 \alpha_t}{r_m} \int_0^{t_f} q' dt . \tag{18}$$

A technique for approximating the above integral by an error function has been developed by H. R. Vaughn.[4] Although developed in order to predict the change in roll rate for a vehicle without roll control, this technique simplifies the calculation of the total impulse requirement of the roll control thrusters.

The approximating function to q' is

$$q' = q'_m \, e^{-a\eta^2} \quad . \tag{19}$$

Since $q'_{max} = 76.5 \times 10^3$ lb/ft^2 at t = 33.0, then

$$\eta = t - 33.0 \text{ seconds}$$

and

$$q'_m = 76.5 \times 10^3 \text{ lb/ft}^2 \quad .$$

In order to compute the value of a, one additional point on the q' versus time curve is chosen arbitrarily. The additional point is $q' = 19.56 \times 10^3$ lb/ft^2 at t = 26 seconds. By substituting these values in Equation 19,

$$19.56 \times 10^3 = 76.5 \times 10^3 \, e^{-a49} \quad ,$$

and

$$a = 0.0278 \text{ per sec}^2 \quad .$$

The approximation to q' is then

$$q' = 76.5 \times 10^3 \, e^{-0.0278\eta^2} \text{ lb/ft}^2 \quad . \tag{20}$$

The approximation to q' is shown, along with q', in Figure 12.

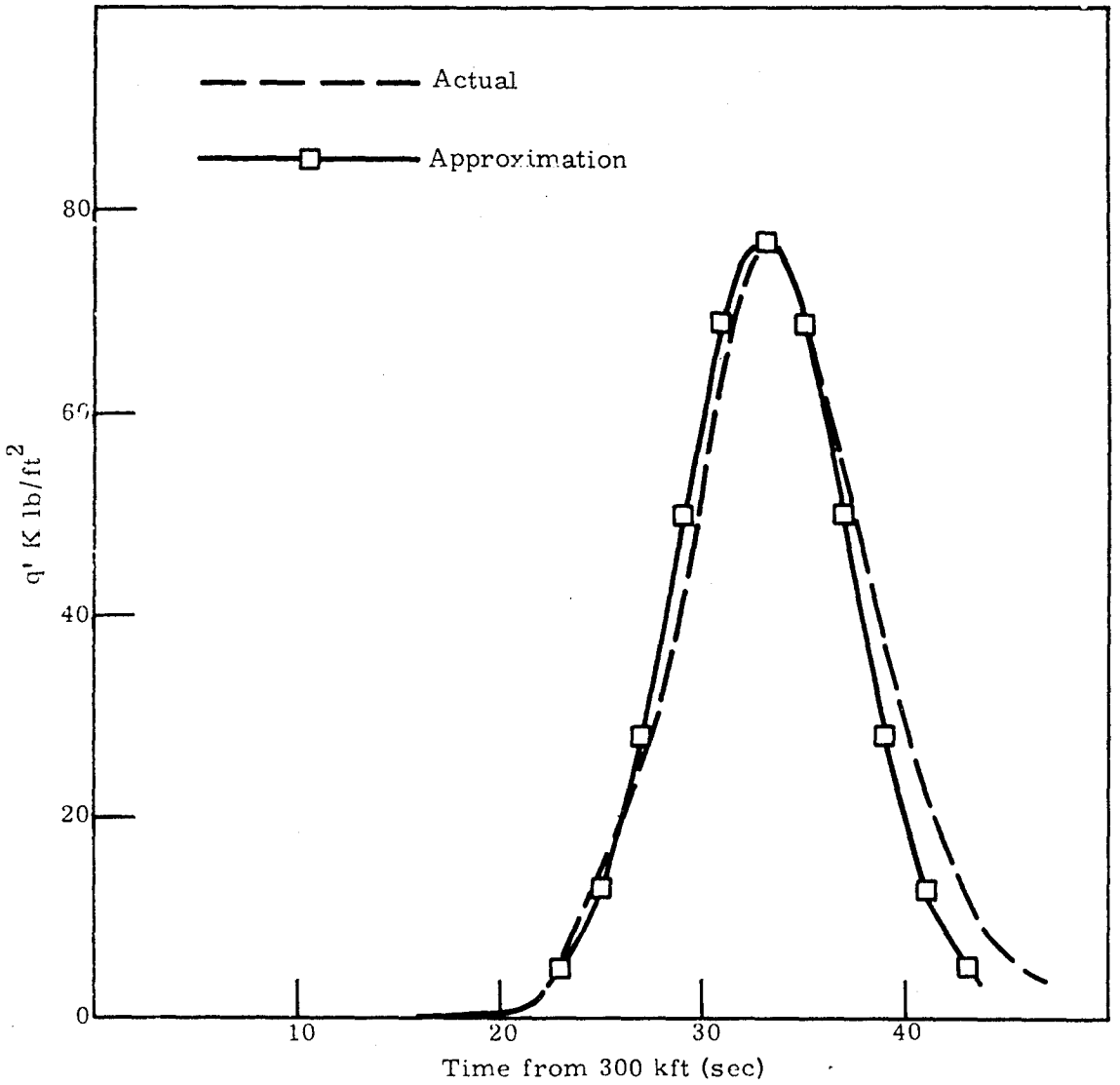

Figure 12. Dynamic Pressure Versus Time

With a change in variables,

$$T^2 = 0.0278\eta^2 ,$$

the integral in Equation 18 may be evaluated as the error function. From

$$T = \sqrt{0.0278}\,\eta ,$$

or

$$T = 0.167(t - 33.0) ,$$

$$dt = 6.0dT ,$$

$$\int_0^{t_f} q'dt = 76.5 \times 10^3 \times 6.0 \int_{-T_f}^{T_f} e^{-T^2} dT . \tag{21}$$

Because q' is small at both time extremes of roll control operation, the above integration may be further simplified by letting

$$T_f \rightarrow +\infty ,$$

and

$$-T_f \rightarrow -\infty ,$$

then since

$$\int_{-\infty}^{+\infty} e^{-T^2} dT = 2 \int_0^{+\infty} e^{-T^2} dT = \sqrt{\pi} , \tag{22}$$

$$\mathscr{I} \geq \frac{C_{N\theta} S y_0 \alpha_t}{r_m} 4.59 \times 10^5 \sqrt{\pi} \text{ lb sec} . \tag{23}$$

Since continuously variable reaction jet thrusters are not practical and because any realizable control system will possess response lags, hysteresis, and dead time, it is not possible to match the control torque to the aerodynamic torque at all times. Therefore the requirement given in Equation 23 is a lower bound on the actual total impulse requirement of a realizable control system.

An upper bound on total impulse may be obtained by noting that, from Figure 12, the time duration of aerodynamic effects for the Castor trajectory chosen is approximately 25 seconds. If two 20-pound thrusters were on continuously during this time, the total impulse would be 500 lb sec.

Basic Control System

A basic roll control system using reaction-jet thrusters and a bang-bang-off controller is shown in Figure 13. The geometric arrangement of the thruster nozzles is shown in Figure 14.

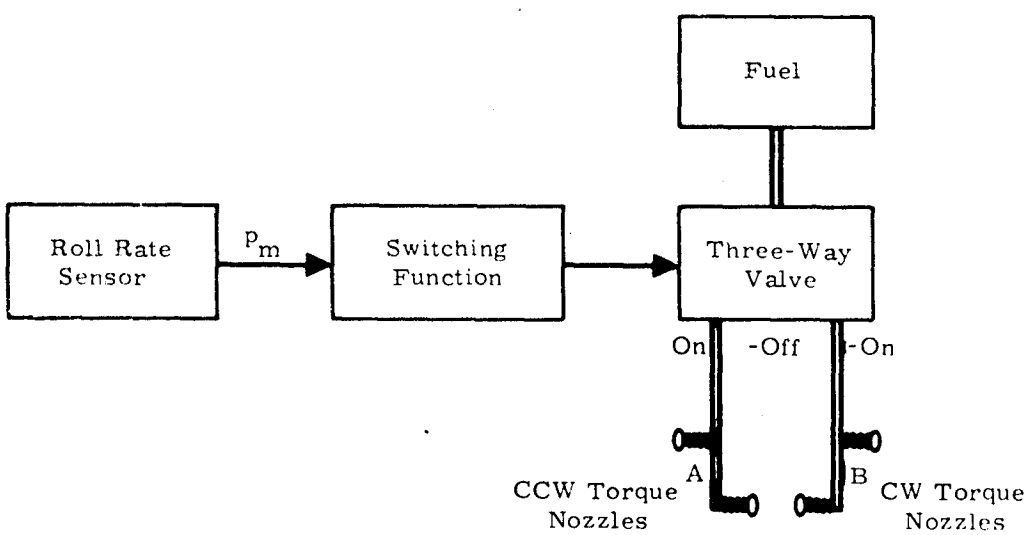

Figure 13. Basic Bang-Bang-Off Roll Control System

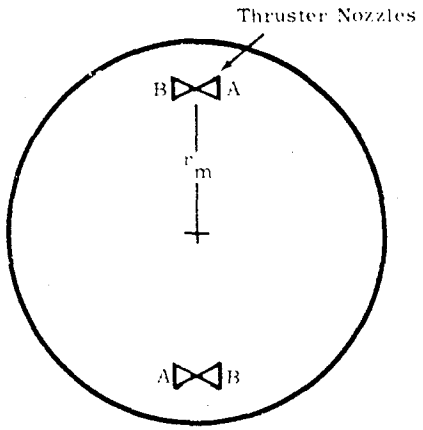

Aft End of RV

Figure 14. Thruster Nozzle Geometry

The roll rate sensor produces a measurement, p_m, of the roll rate, and the switching function then determines whether one of the pairs of thrusters must be turned on in order to control the roll rate, p.

Switching Function Analysis

Since the objective of the roll control system is to prevent instabilities in the roll behavior of the RV and large impact dispersions caused by flight through zero roll rate, the roll rate must be confined to a band of values (p_L to p_H) which does not include zero. Therefore, the switching function output must be a three-leveled logic signal (Figure 15a).

If there exists a positive or negative aerodynamic induced torque, the control system will chatter against the upper or lower boundary of the permissible band (turning the fuel valve on and off at a high frequency). In order to prevent this undesirable behavior, hysteresis (dead time) or response lag may be added to the design of the controller. Often these factors are inherent in the control and thruster components themselves. Figure 15b indicates a switching function with hysteresis.

Switching Function Hysteresis

The input to the switching function is the continuous measurement, p_m, of the roll rate, p. The output is the three-leveled logic shown in Figure 15. However, the switching point in going from $p_L < p < p_H$ to either $p < p_L$ or to $p > p_H$ may not be the same as when going from $p < p_L$ to $p_L < p < p_H$ or from $p > p_H$ to $p_L < p < p_H$. This hysteresis is shown in Figure 15b. The role of switching hysteresis in obtaining desirable control system behavior will be analyzed in a later section.

In order to analyze the control system with hysteresis, the Laplace transform of Equation 6 may be taken for the case $p \neq \dot{\psi}$ (so that the term $\theta \sin \phi$ may be neglected), and a fixed value of N_θ may be assumed (where this fixed, time invariant value may be chosen to correspond to any point in the trajectory); therefore,

$$sP(s) - p(0) = -\frac{N_\theta y_0 \alpha_t}{I_x s} + \frac{L_u u}{I_x s} . \tag{24}$$

If the control system is assumed to be off (u = 0), $p(0) = p_c$, α_t negative, and $y_0 \neq 0$; the time, T_1, required to go from p_c to p_d is found from

$$P(s) = \frac{1}{s}\left(p_c - \frac{N_\theta y_0 \alpha_t}{sI_x}\right) , \tag{25}$$

therefore,

$$p(t) = p_c - \frac{N_\theta y_0 \alpha_t}{I_x} t , \tag{26}$$

and

$$T_1 = \left\{\frac{(p_d - p_c)I_x}{-N_\theta y_0 \alpha_t}\right\} . \tag{27}$$

At $p = p_d$ the control system turns on ($u = -1$) and the time, T_2, required to go from p_d back to p_c is

$$T_2 = \left\{\frac{(p_d - p_c)I_x}{N_\theta y_0 \alpha_t + L_u}\right\} . \tag{28}$$

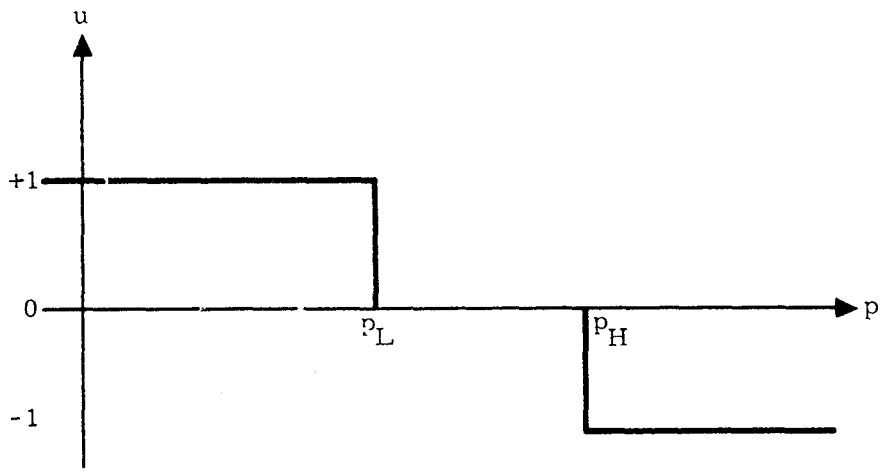

Figure 15a. Switching Function Output

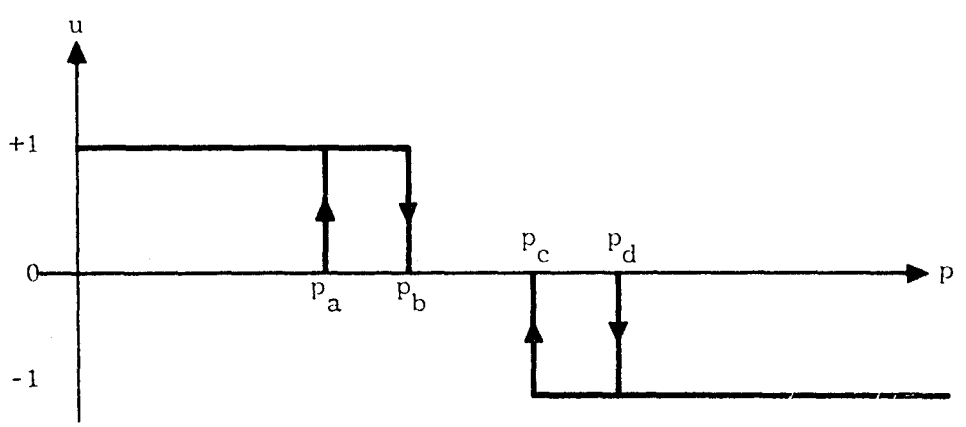

Figure 15b. Switching Function Output with Hysteresis

From the above analysis, the on-time of the thruster is directly proportional to the amount of hysteresis $(p_d - p_c)$. When $|N\ y_0\alpha_t| > L_u$, the amount of thrust developed by the control system is insufficient to counter the aerodynamic torques, and the vehicle will roll up or roll reverse at a rate proportional to the difference of the aerodynamic and control torques.

If Equations 27 and 28 are used, the on-and-off time of the thruster may be designed by proper choice of $(p_d - p_c)$ for the particular thruster and thruster valve chosen.

Switching Function Dead Time

The following analysis is treated for the case $\alpha_t < 0$ which results in spinup. Roll reversal $(\alpha_t > 0)$ can be handled in a completely analogous fashion. So far it has been assumed that if p is increasing and $p = p_d$ at $t = t_0$, then $u = -1$ at $t = t_0$. If, however, there is some dead time, T_{sd}, then $u = 0$ at $t = t_0$ and $u = -1$ at $t = t_0 + T_{sd}$.

Dead time affects the switching times T_1 and T_2 in the following way. Assume that the system is in the state $p = p_c$ at $t = 0$, $u = 0$ and α_t is negative. The time required to go to the state p_d is T_1; however, when $p = p_d$, at $t = T_1$, u remains the same, i.e., $u = 0$.

Only at $t = T_1 + T_{sd}$ does the thruster finally come on, i.e., $u = -1$. During the time interval T_{sd}, the roll rate has increased by

$$p^{+}_{T_{sd}} = -\left(\frac{N_\theta y_0 \alpha_t}{I_x}\right) T_{sd} \text{ rad/sec} . \tag{29}$$

Assume now that the system is in the state $p = p_d$ at $t = 0$, $u = -1$, and α_t is negative. The time required to go to the state p_c is T_2; however, when $p = p_c$, at $t = T_2$, u remains at $u = -1$.

Only at $t = T_2 + T_{sd}$ will $u = 0$. The roll rate decrease during the interval T_{sd} is

$$p^{-}_{T_{sd}} = -\left(\frac{N_\theta y_0 \alpha_t + L_u}{I_x}\right) T_{sd} . \tag{30}$$

If

$$\bar{p}_{Tsd} \geq p_c - p_a \,, \tag{31}$$

at $T_2 + T_{sd}$, the control system will turn on again (T_{sd} seconds later), and aid the aerodynamic torque and force the system into an undesirable limit cycle where the roll rate is forced from one extreme of the control band to the other until the fuel is exhausted.

The boundary condition for this dead time instability may be obtained from Equations 30 and 31.

$$p_c - p_a \leq -\left(\frac{N_\theta y_0 \alpha_t + L_u}{I_x}\right) T_{sd} \,. \tag{32}$$

Note that this condition may be satisfied if either T_{sd} or L_u is large. Therefore, an upper bound on T_{sd} and/or L_u is a necessary condition.

The thruster valve off time is

$$T_{valve\ off} = T_1 + T_{sd} \,, \tag{33}$$

and

$$T_{valve\ on} = T_2 + T_{sd} \,. \tag{34}$$

Thruster Characteristics

Reaction jet thrusters, utilizing cold gas or liquid monopropellant, may be modeled by the following first-order differential equation:

$$\frac{df(t - T_{Td})}{dt} + \frac{1}{\tau} f(t - T_{Td}) = \frac{1}{\tau} F_0 u \,. \tag{35}$$

The time delay, from thruster valve turn-on ($|u| = 1$) to fuel reaching the nozzle, is modeled as a dead time, T_{Td}. The thrust versus time output of the nozzle is modeled as the differential equation with time constant τ, final value F_0, and no time delay. The input-output characteristics of the thruster are shown in Figure 16.

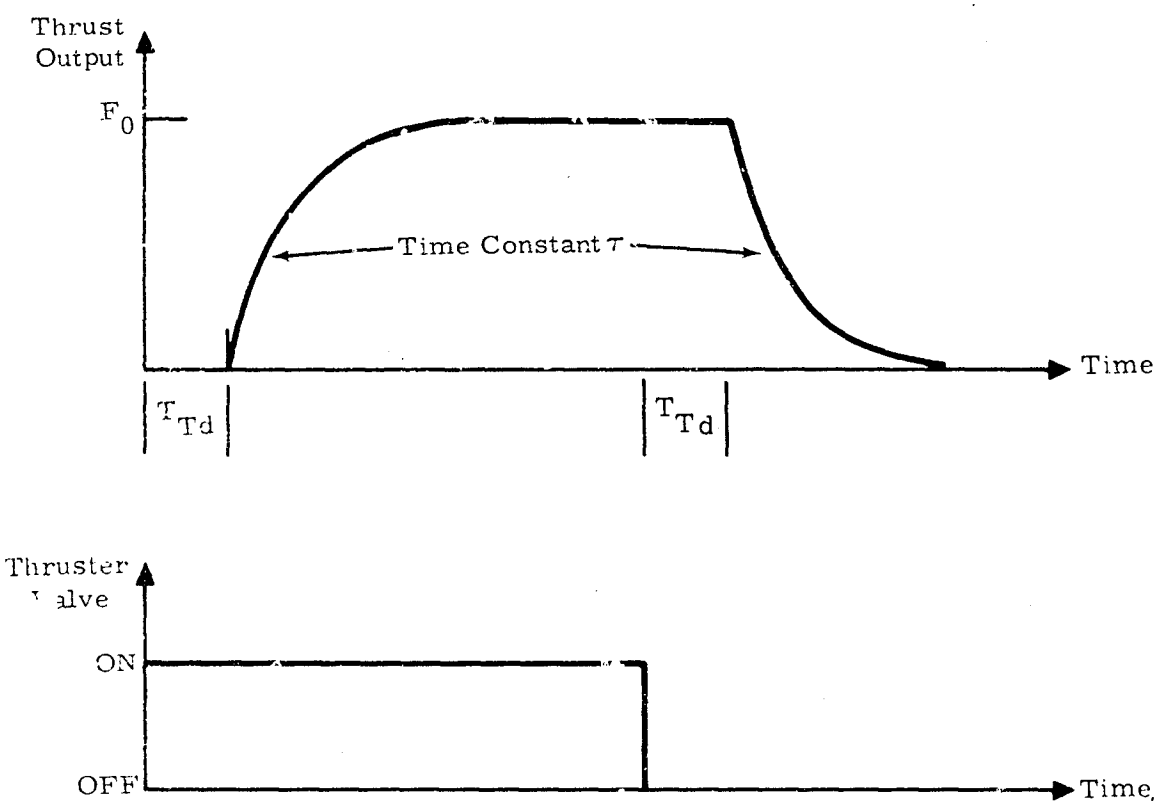

Figure 16. Thruster Input-Output Characteristics

The effects of time delay and lag may be separated in Equation 35 by taking Laplace transforms:

$$e^{-sT_{Td}} \left\{ sF(s) + \frac{1}{\tau} F(s) \right\} = \frac{1}{\tau} F_0 \frac{u}{s} \tag{36}$$

Figure 17 shows the complete model of the control system, including thruster and switching characteristics.

The thrust output, $F(s)$, is multiplied by $2r_m$ in order to obtain the control torque from two thrusters with moment arm r_m from the centerline of the vehicle (Figure 14).

Since T_{TD} appears as a series time delay in the control system, it has been lumped together with the switching delay T_{sd}. If, in addition, the sensor has time delay T_{ad}, then the total dead time of the system may be represented by

$$e^{-s(T_{ad}+T_{sd}+T_{Td})} .$$

The analysis of the valve switching time and dead time stability may then be performed as outlined under Switching Function Dead Time.

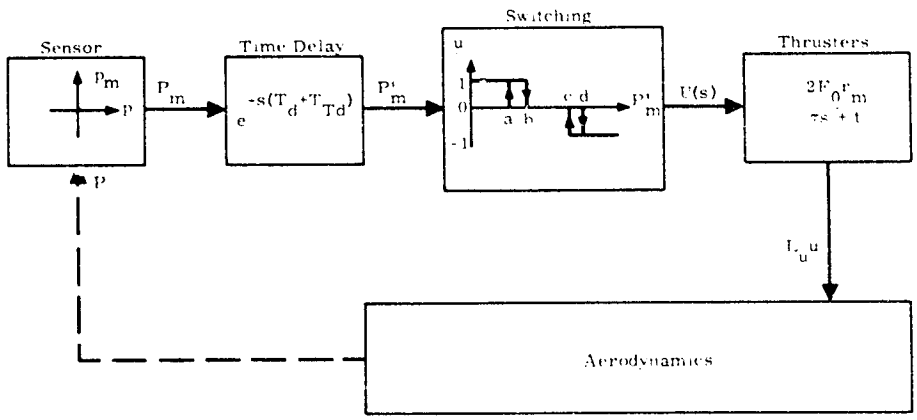

Figure 17. Complete Roll Control System Model

Limit Cycle Behavior with Thruster Lag and Zero Dead Time

If $T_{Td} = 0$ second and $p \neq \dot{\psi}$ are assumed, Equations 2 and 35 may be used to construct the phase plane portrait of thrust output, f, versus roll rate, p. Since $p \neq \dot{\psi}$, the term $N_\theta \theta_{y0} \sin \phi$ is oscillatory with a frequency given approximately by $p - \dot{\psi}$; it therefore has zero average value. For small θ and $\dot{\psi} > p$, $N_\theta \theta_{y0} \sin \phi$ is a high frequency low amplitude perturbation in the roll equation and will therefore be ignored.

The slope of the f versus p curve is given at each point by

$$\frac{df}{dp} = \frac{I_x(uF_0 - f)}{\tau(2r_m f - N_\theta y_0 \alpha_t)} . \tag{37}$$

Equation 37 forms the basis of the isocline method;[7] by plotting the slope at a sufficient number of points, the phase plane portrait of f versus p may be obtained.

System Phase Plane Portrait

The parameter values given in Table I with $r_m = 0.5$ ft, $\alpha_t = -1.0$ degree, $y_0 = 0.005$ ft, $T = 0.05$ second, $F_0 = 10$ lb, and with $q' = 60,000$ lb/ft^2 are used to present the phase plane portrait given in Figure 18. Note that this figure displays a stable limit cycle about the hysteresis characteristic of p'_m. The open arrows in the figure represent the system with the thrusters on ($u = +1$ or -1), while the closed arrows represent the system with the thrusters off ($u = 0$).

The time required to go from point 1 to 3 along the path 1-2-3 is found from

$$p_c - p_d = \int_0^{T_{on}} \frac{\left(-N_\theta y_0 \alpha_t + 2r_m f(t)\right)}{I_x} dt , \tag{38}$$

and with

$$f(t) = -F_0(1 - e^{-t/\tau}) , \tag{39}$$

and $r_m = 0.5$ feet,

$$p_c - p_d = -\frac{N_\theta y_0 \alpha_t T_{on}}{I_x} - \frac{F_0 2r_m}{I_x}\left(T_{on} + \tau e^{-T_{on}/\tau} - \tau\right) . \tag{40}$$

Assuming $\tau < T_{on}$, Equation 40 may be simplified to

$$T_{on} = \frac{I_x(p_d - p_c)}{N_\theta y_0 \alpha_t + F_0 2r_m} . \tag{41}$$

With the constant values used in the example, $T_{on} = 0.31$ second. The time required to go from point 3 to 1 along the path 3-4-1 may be found by using

$$p_d - p_c = \int_0^{T_{off}} \frac{\left(-N_\theta y_0 \alpha_t + 2r_m f(t)\right)}{I_x} dt , \tag{42}$$

[redacted]

UNCLASSIFIED

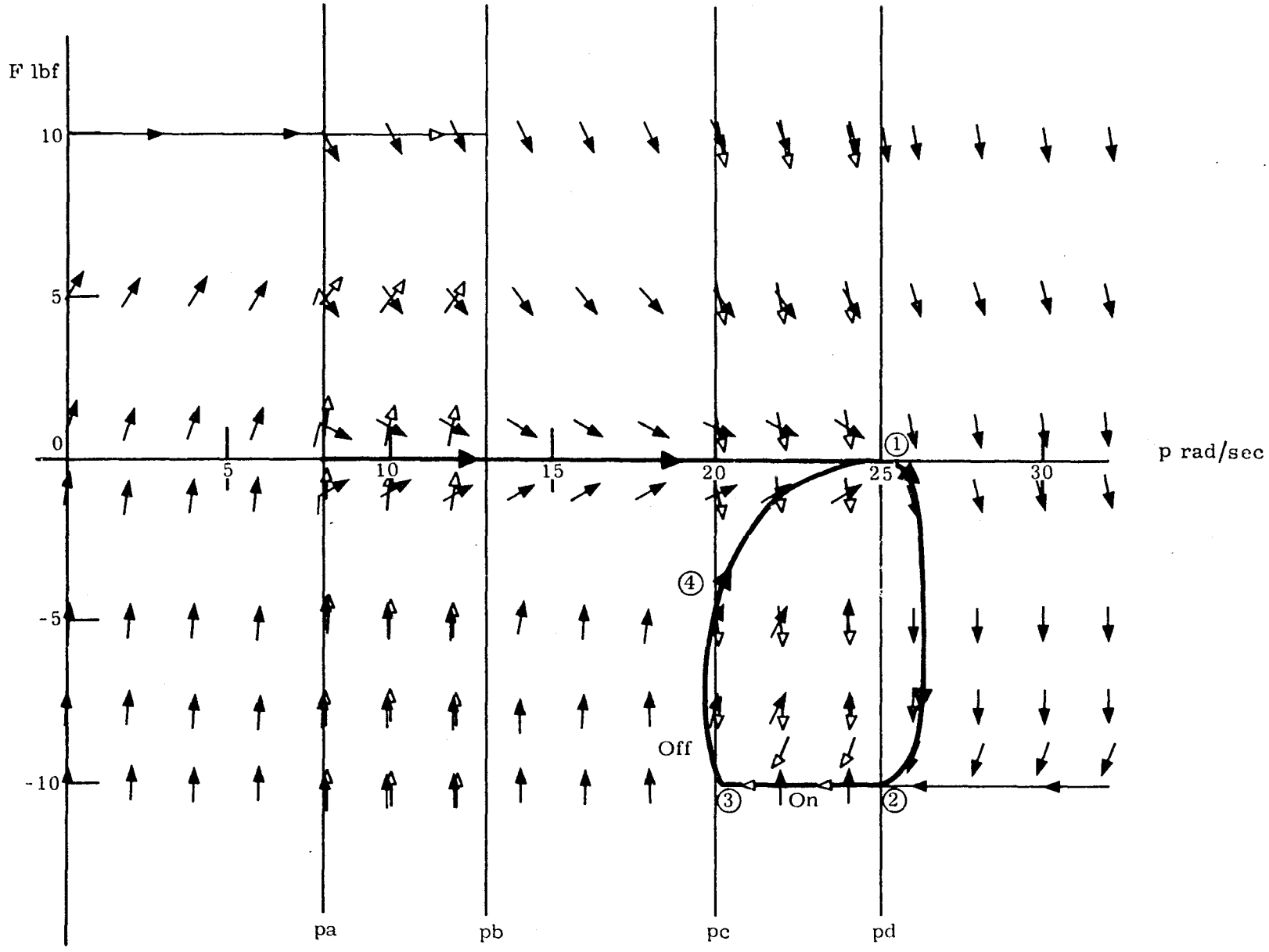

Figure 18. Phase Plane Portrait ($q' = 60,000$ lb/ft^2)

[redacted]

UNCLASSIFIED

however, in this instance

$$f(t) = -F_0 \, e^{-t/\tau}. \tag{43}$$

Evaluating the integral in Equation 42 and simplifying,

$$T_{off} = \frac{I_x(p_d - p_c) + F_0 \tau 2 r_m}{-N_\theta y_0 \alpha_t} \tag{44}$$

For the example, in Figure 18,

$$T_{off} = 0.425 \text{ second} \; .$$

Figure 19 is the phase plane portrait when $q' = 20,000 \text{ lb/ft}^2$. For this case

$$T_{on} = 0.13 \text{ second} \; ,$$

and

$$T_{off} = 0.88 \text{ second} \; .$$

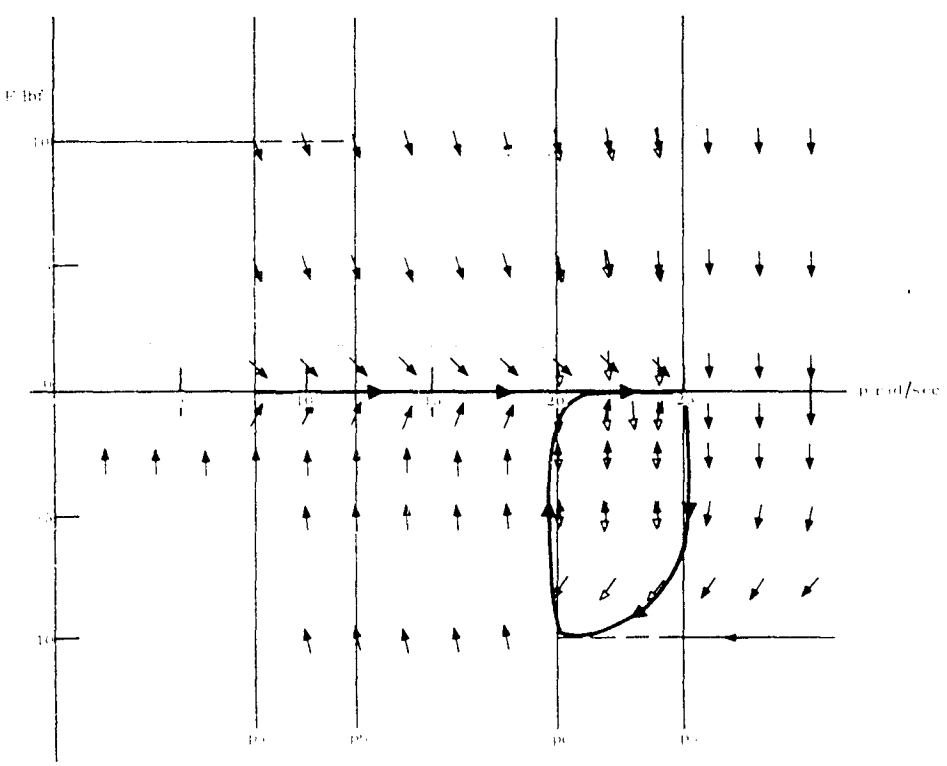

Figure 19. Phase Plane Portrait ($q' = 20,000 \text{ lb/ft}^2$)

As expected, the thruster on-time is less when the dynamic pressure is small, and the thruster off-time is inversely proportional to the dynamic pressure.

The analog computer may be programmed to produce the phase plane portraits for the case of variable q' during reentry. Figure 20 shows such a plot. Note the excellent correspondence between the analog phase portraits and those obtained by the isocline method. The time savings in using the analog over the hand-worked isocline method is approximately a factor of 15. However, the analog computer, and for that matter the digital simulation codes, is only valuable as a tool when coupled with analysis and a fundamental understanding of the control and dynamical system.

Undesirable Limit Cycles

As in the case of dead time instability examined previously, an undesirable limit cycle may exist if either the thrust level or lag time constant is too high.

The sketch of an undesirable limit cycle is shown in Figure 21.

Assume that the system is in state $p = p_d$, $f = 0$, and u has just switched from 0 to -1 at time $t = 0$. At time $t = T_c$, $p = p_c$; u switches to 0, and $f = F_c$. T_c and F_c may be found by using

$$(p_c - p_d) = \int_0^{T_c} \frac{- N_\theta \alpha_t y_0 - F_0 2 r_m (1 - e^{-t/\tau})}{I_x} \, dt \, , \tag{45}$$

and

$$F_c = -F_0 \left(1 - e^{-T_c/\tau}\right) . \tag{46}$$

Assuming the thrust level F_0 or lag time constant τ is too high $T_c < \tau$ and Equation 45 may be solved for T_c yielding

[redacted]

UNCLASSIFIED

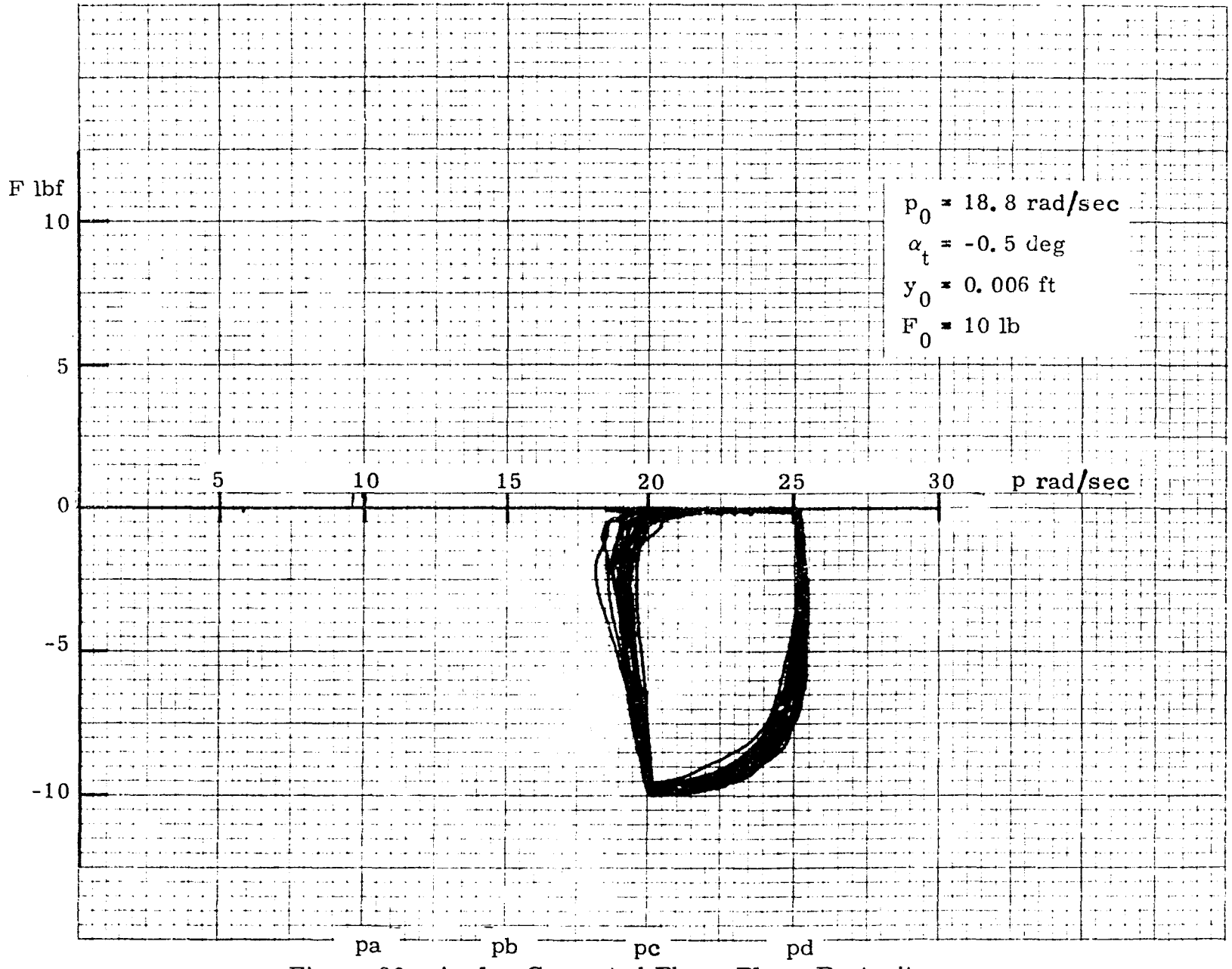

Figure 20. Analog Generated Phase Plane Portrait

[redacted]

UNCLASSIFIED

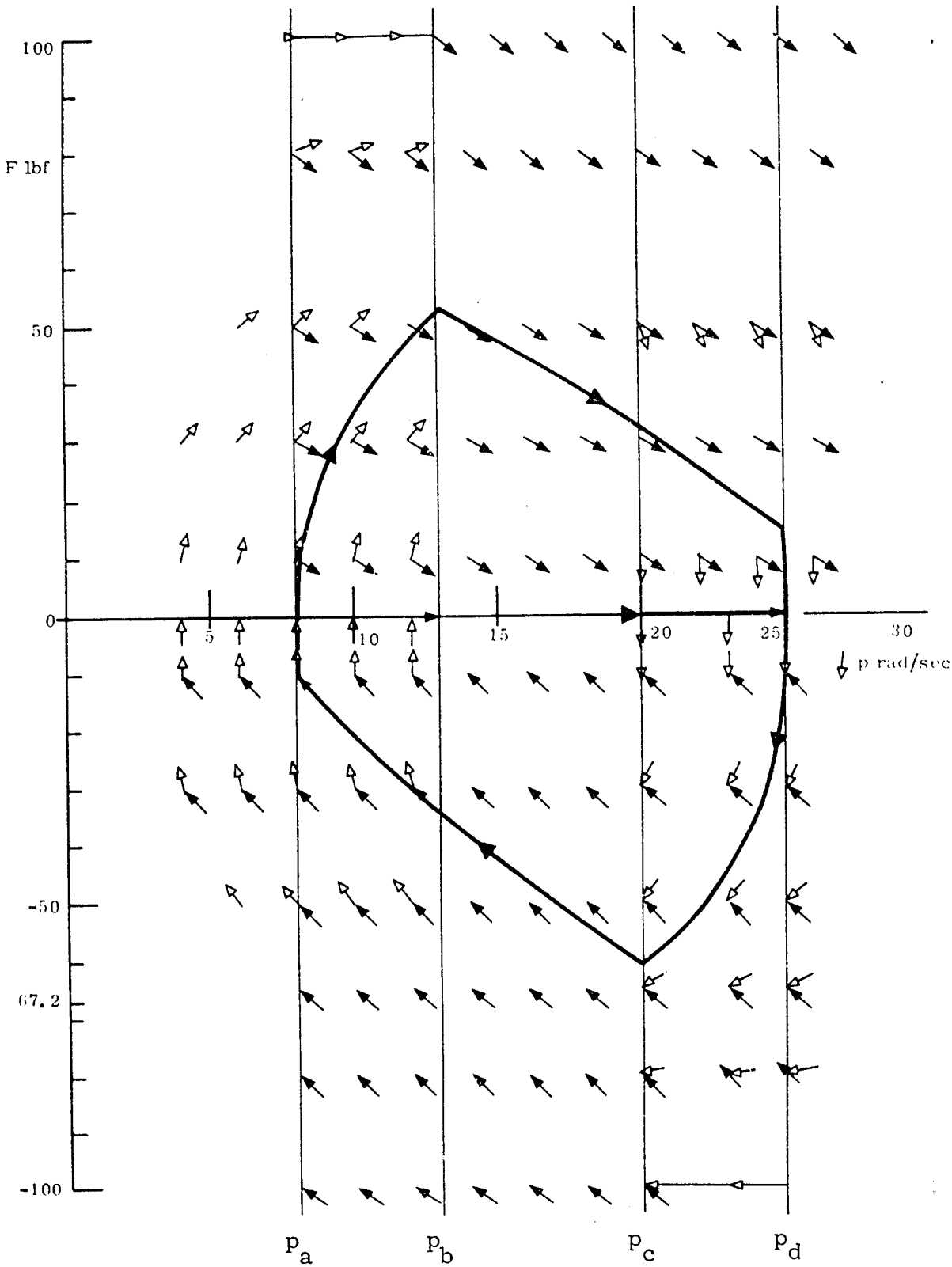

Figure 21. Undesirable Limit Cycle

$$T_c \approx -\frac{\tau N_\theta \alpha_t y_0}{F_0 2r_m} + \sqrt{\left(\frac{\tau N_\theta \alpha_t y_0}{F_0 2r_m}\right)^2 + \frac{2\tau I_x (p_d - p_c)}{F_0 2r_m}} \ . \tag{47}$$

Assuming now that

$$\frac{2\tau I_x}{F_0 2r_m}(p_d - p_c) \gg \left(\frac{\tau N_\theta \alpha_t y_0}{F_0 2r_m}\right)^2 , \tag{48}$$

then

$$T_c \approx \left\{\frac{2\tau I_x}{F_0 2r_m}(p_d - p_c)\right\}^{1/2} , \tag{49}$$

and

$$F_c \approx -F_0 \frac{T_c}{\tau} \ . \tag{50}$$

For example, if $\tau = 0.05$ sec, $p_d - p_c = 5$ rad/sec, and $F_0 = 100$ lb/ft, then $T_c \approx 0.034$ second, and $F_c \approx -68$ lbf. Indeed, $T_c < \tau$ and the assumption made in Equation 48 is verified since $11.25 \times 10^{-4} \gg 3.67 \times 10^{-6}$.

After the thrusters turn off, the thrust output decays per Equation 43. When the decaying thrust level equals the aerodynamic torque, the vehicles' roll rate will cease to decrease and begin to increase due to the aero-induced torque. Assume the decaying thrust level equals the aerodynamic torque at $t = T^*$ seconds after thruster turnoff. This may be expressed as

$$-N_\theta y_0 \alpha_t = 2r_m F_c \, e^{-T^*/\tau} , \tag{51}$$

or

$$T^* = \tau \ln \frac{F_c 2r_m}{-N_\theta y_0 \alpha_t} \ . \tag{52}$$

If $p \leq p_a$ at $t = T^*$, the control system will turn on the thruster in a direction aiding the aerodynamic torque, and an undesirable limit cycle similar to that examined previously for the case of dead time instability will result.

The boundary conditions for the existence of this undesirable limit cycle is

$$(p_c - p_a) \leq \int_0^{T^*} \frac{\left(N_\theta \alpha_t y_0 - 2r_m F_c e^{-t/\tau}\right)}{I_x} dt \ . \tag{53}$$

Using Equations 50 and 52 in the evaluation of the above integral yields

$$I_x(p_c - p_a) \leq N_\theta \alpha_t y_0 \tau \left\{1 + \ln\left(\frac{-\xi^{1/2}}{N_\theta \alpha_t y_0 \tau}\right)\right\} + \xi^{1/2} \ , \tag{54}$$

where

$$\xi = 2\tau F_0 2r_m I_x (p_d - p_c) \ . \tag{55}$$

The boundary condition given in Equations 54 and 55 may be used for the existence of the undesirable limit cycle given α_t, y_0, τ, and F_0. Note that satisfaction of this boundary condition is consistent with a high thrust level, F_0, a long decay time constant, τ, and small compound asymmetries, $\alpha_t y_0$.

Limit Cycle Behavior with Thruster Lag and Nonzero Dead Time

Nonzero dead time may be added to the previous analysis by modifying Equation 46 to include the additional dead time, T_D (assuming the change in roll rate due to the aerodynamic torque is small during the time interval T_D):

$$F_c = -F_0\left[1 - e^{-(T_c - T_D)/\tau}\right] . \tag{56}$$

If $T_c + T_D > \tau$ then

$$F_c \approx -F_0 \, , \tag{57}$$

and Equation 52 becomes

$$T^* \approx \tau \ln - \frac{F_0 2 r_m}{N_\theta t_0 \alpha_t} \, . \tag{58}$$

If $p \leq p_a$ at $t = T^*$ then the wrong control thrusters will turn on, as in the case of undesirable limit cycles with thruster lag at $t = T^* + T_D$.

The boundary condition for the existence of this undesirable limit cycle is

$$p_c - p_a \leq \int_0^{T^*} \frac{\left(N_\theta \alpha_t y_0 + 2 r_m F_0 \, e^{-t/\tau}\right)}{I_x} \, dt \, , \tag{59}$$

where

$$p_c = p_c - \frac{F_0 2 r_m T_D}{I_x} \, . \tag{60}$$

The boundary condition is then

$$I_x (p_c - p_a) - F_0 2 r_m T_D \leq F_0 2 r_m \tau + N_\theta \alpha_t y_0 \tau \left\{ \ln - \left(\frac{F_0 2 r_m}{N_\theta y_0 \alpha_t} \right) - 1 \right\} . \tag{61}$$

Design Examples

The following numerical examples demonstrate applications of the analytical tools developed in this study.

Example 1: Peak Torque When $p = \dot{\psi}$ -- With $p_{initial}$ = 3 rps, y_0 = 0.12 inch (0.01 foot), and $(\theta - \alpha_t)$ = 5 degrees, then from Figure 5 $p = \psi$ at approximately 20 seconds from 300 kilofeet. The nominal dynamic pressure at this time is 2.65×10^3 lb/ft^2, and from relation 9a,

$$N_\theta = C_{N\theta} S q' \ .$$

With these values in Equation 13,

$$L_{ax\,peak} = 2.5 \times 10^{-2} \times 0.852 \times 2.654 \times 10^3 \times 0.01 \times 5 \text{ ft lb} \ ,$$

or

$$L_{ax\,peak} = 2.82 \text{ ft lb} \ .$$

Example 2: Peak Torque When $p = \dot{\psi}$ -- With $p_{initial}$ = 8 rps, y_0 = 0.12 inch, and $(\theta - \alpha_t)$ = 5 degrees, then $p = \dot{\psi}$ at approximately 25.5 seconds from 300 kilofeet. The nominal dynamic pressure at this time is 17.0×10^3 lb/ft^2; therefore,

$$L_{ax\,peak} = 25 \times 10^{-2} \times 0.852 \times 17.0 \times 10^3 \times 0.01 \times 5 \text{ ft lb} \ ,$$

or

$$L_{ax\,peak} = 18.1 \text{ ft lb} \ .$$

Note that the value of $L_{ax\,peak}$ is a sensitive function of the initial roll rate, since the time at which $p = \dot{\psi}$ determines the value of q' which must be entered into Equation 13. Thus by proper choice of $p_{initial}$, the peak torque required when $p = \dot{\psi}$ can be minimized.

The maximum average torque required, from Equation 12, occurs when N_θ is a maximum. Since $N_\theta = C_{N\theta} S q'$, N_θ max occurs when q' is a maximum. From Figure 3, q' max occurs at t = 33 seconds.

Thus the maximum value $L_{ax}DC$ is given by

$$L_{ax}DC = -2.5 \times 10^{-2} \times 0.852 \times 76.5 \times 10^{3} \times y_0 \times \alpha_t \text{ ft lb} .$$

Example 3: Maximum Average Torque -- If $y_0 = 0.01$ foot (0.12 inch) and $\alpha_t = -1$ degree are used in Equation 12,

$$L_{ax}DC = 16.3 \text{ ft lb} .$$

Example 4: Total Impulse -- Assume

$$C_{N\theta} = 2.5 \times 10^{-2} \text{ per degree}$$

$$S = 0.852 \text{ ft}^2$$

$$r_m = 0.5 \text{ ft}$$

$$y_o = 0.01 \text{ ft (0.12 inch)}$$

$$\alpha_t = 1.0 \text{ degree} .$$

Then the total impulse obtained from Equation 23 is

$$\mathscr{I} = 346 \text{ lb sec} .$$

If a fuel, such as hydrazine, with a specific impulse of approximately 210 lb sec/lbm is used, then at least 1.65 lbm of fuel is required.

Example 5: Switching Time with Control Hysteresis -- Assume

$p_d = 25$ rad/sec

$p_c = 20$ rad/sec

$L_u = 20$ lb ft

$\alpha_t = -1.0$ degree

$y_o = 0.01$ ft (0.12 inch)

$S = 0.852$ ft^2

$C_N = 2.5 \times 10^{-2}$ per degree

$I_x = 0.225$ slug ft^2 .

Case 1

When $q' = 35,000$ lb/ft^2, Equations 27 and 28 yield

$T_1 = 0.151$ sec ,

and

$T_2 = 0.0897$ sec .

Case 2

When $q' = 70,000$ lb/ft^2, Equations 27 and 28 yield

$T_1 = 0.0755$ sec ,

and

$T_2 = 0.221$ sec .

Example 6: Roll Rate Increase During Switching Dead Time -- For

$$y_0 = 0.01 \text{ ft}$$

$$\alpha_t = -1.0 \text{ degree}$$

and with the constants from Table I, Equation 29 yields

$$p^+_{Tsd} = 33.1 T_{sd} \text{ rad/sec} ,$$

and for

$$T_{sd} = 0.030 \text{ second} ,$$

$$p^+_{Tsd} = 0.993 \text{ rad/sec} .$$

Thus the roll rate increase is proportional to the dead time, and with small dead time ($T_{sd} \leq 0.03$ second) the increase in p is negligible.

Example 7: Dead Time Instability -- For

$$y_0 = 0.01 \text{ ft}$$

$$\alpha_t = -1.0 \text{ degree}$$

and with the constants from Table I, Equation 32 yields

$$p_c - p_a \leq -\left(\frac{7.46 + L_u}{0.225}\right) T_{sd}$$

and for

$$T_{sd} = 0.03 \text{ second} ,$$

$$p_c - p_a = 12 \text{ rad/sec} .$$

Therefore, $L_u \geq 97.5$ lb ft will result in the undesirable limit cycle behavior.

Example 8: Undesirable Phase Plane Portrait -- Asume that $F_0 = 100$ lb/ft, $\tau = 0.05$ sec, $\alpha_t = 0.5$ degree, $y_0 = 0.005$ ft, and $q' = 60,000$ lb/ft^2. Then the boundary condition given in Equations 54 and 55 is satisfied, since $1.125 \leq 3.676$.

The phase plane portrait of this example is given in Figure 21.

Example 9: Undesirable Phase Plane Portrait -- Assume a roll control design using $F_0 = 80$ lb/ft, $\tau = 0.05$ sec, $\alpha_t = 0.5$ degree, $y_0 = 0.005$ ft, $q' = 60,000$ lbf/ft^2, and $T_D = 0.02$ sec. The boundary condition in Equation 61 is satisfied, because $1.1 \leq 4 - 0.353$.

The design in this example is therefore unsatisfactory; for, although this system provides a high enough control torque, the fuel consumption would be enormous because of the high total impulse (800 lbf sec) which would result from the undesirable limit cycle.

Analog Simulation of Roll Control Systems

Figures 22 through 27 display the analog computer simulation of the RV aerodynamic model (Equations 6, 7, 8, 9, and 10) with programmed dynamic pressure (Figure 3) and velocity (Figure 4). The block diagram of the roll control system studied is given in Figure 17. The following parameter values were used:

$P_m = P$ rad/sec

$T_D = T_{TD} = 0$ sec

$p_a = 8$ rad/sec

$p_b = 13$ rad/sec

$p_c = 20$ rad/sec

$p_d = 25$ rad/sec

$\tau = 0.05$ sec.

Various values of α_t, y_0, and F_0 were used to investigate the behavior of the RV model with roll control. A brief resumé of each simulation will now be correlated with the analysis in this paper.

Figure 22

Assume

$y_0 = 0.002$ ft

$\alpha_t = -0.0087$ rad .

Equation 12 requires that $2r_mF_0 > 1.63$ lb ft; therefore, $2r_mF_0 = 10$ lb was used. Equation 23 requires that $I > 35$ lb sec. Analog integration of the simulation yielded $\mathcal{I}_{sim} = 48$ lb sec.

The roll rate limit cycle behaved as the analysis predicted.

Figure 23

Assume

$y_0 = 0.005$ ft

$\alpha_t = 0.0174$ rad.

Equation 12 requires $2r_mF_0 > 8.15$ lb ft; therefore, $2r_mF_0 = 10$ lb ft was used. Equation 23 requires $I > 174$ lb sec; therefore, $\mathcal{I}_{sim} = 204$ lb sec was obtained.

The control system performed satisfactorily, although some slight increase in peak roll rates occurred when dynamic pressure was maximum.

Figure 24

Assume

$y_0 = 0.01$ ft

$\alpha_t = -0.0174$ rad.

Equation 12 requires that $2r_mF_0 > 16$ lb ft; only $2r_mF_0 = 10$ lb ft was used, and the vehicle spun up as expected when the aerodynamic roll torque exceeded the control.

Figure 25

This figure was similar to Figure 24 but with $2r_mF_0 = 20$ lb ft. The system performed satisfactorily and corresponded excellently with the analysis.

Figure 26

Assume

$y_0 = 0.002$ ft

$\alpha_t = 0.0087$ rad.

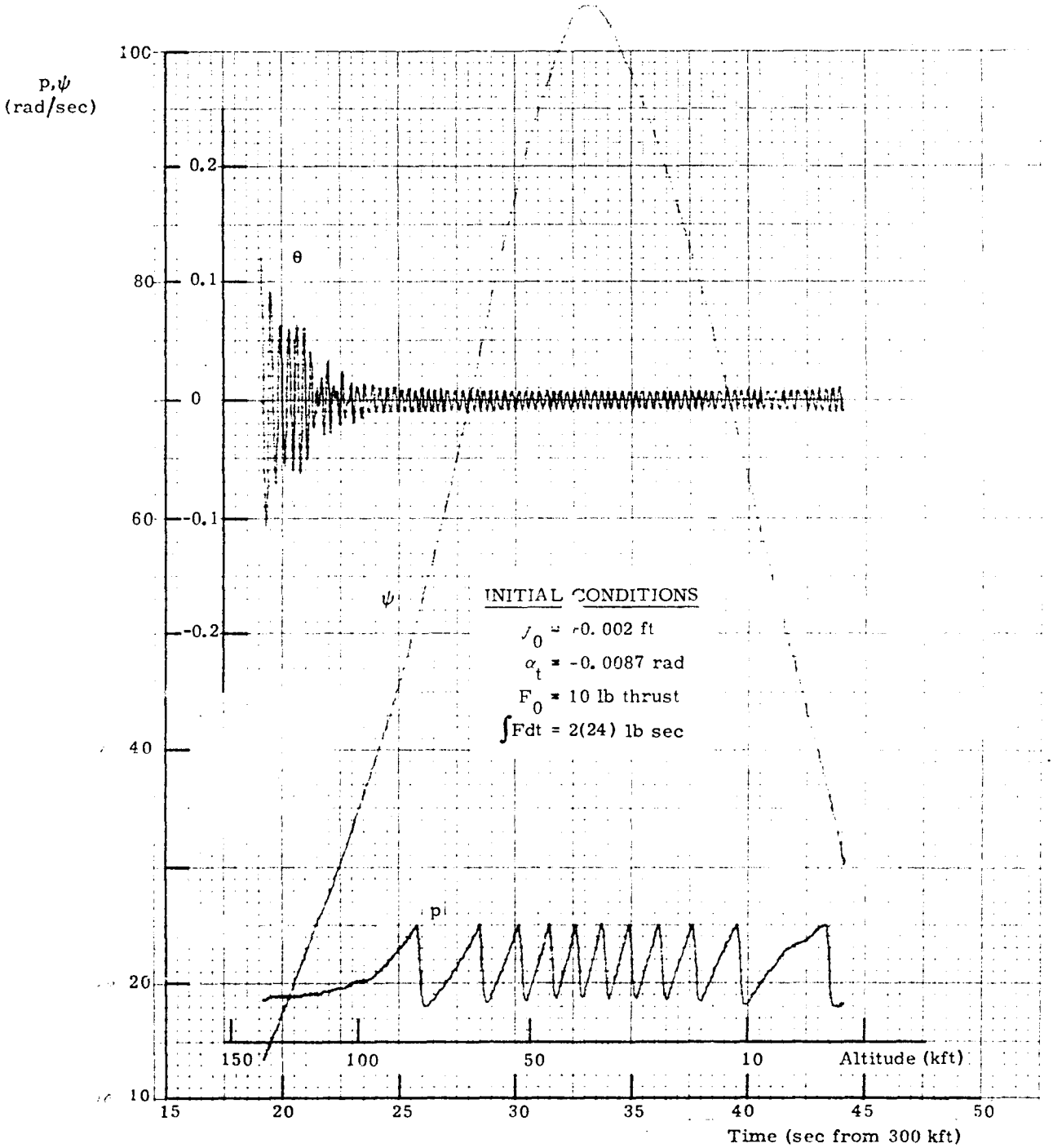

Figure 22. Analog Simulation with Roll Control (Small Asymmetries)

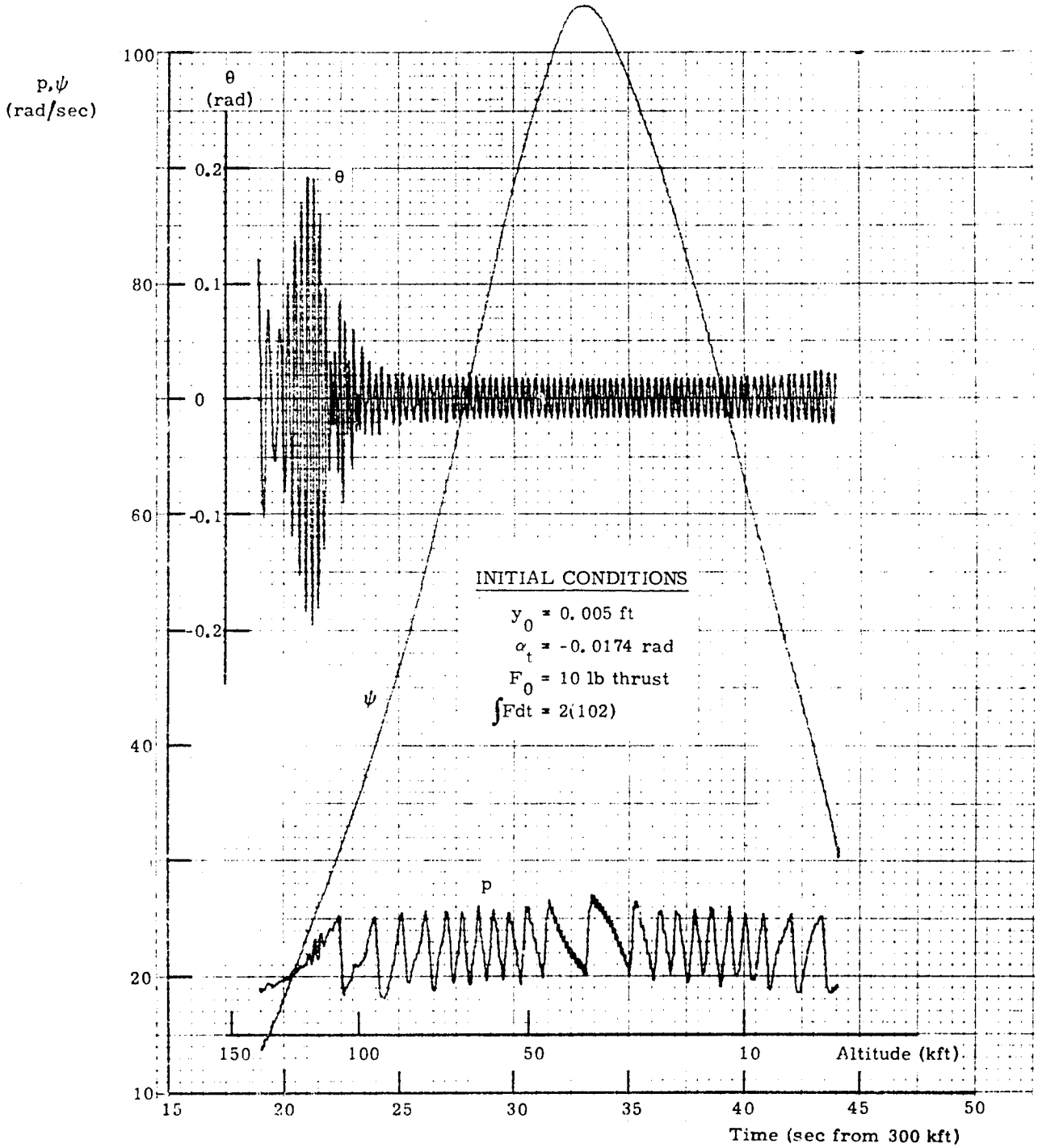

Figure 23. Analog Simulation with Roll Control (Nominal Asymmetries)

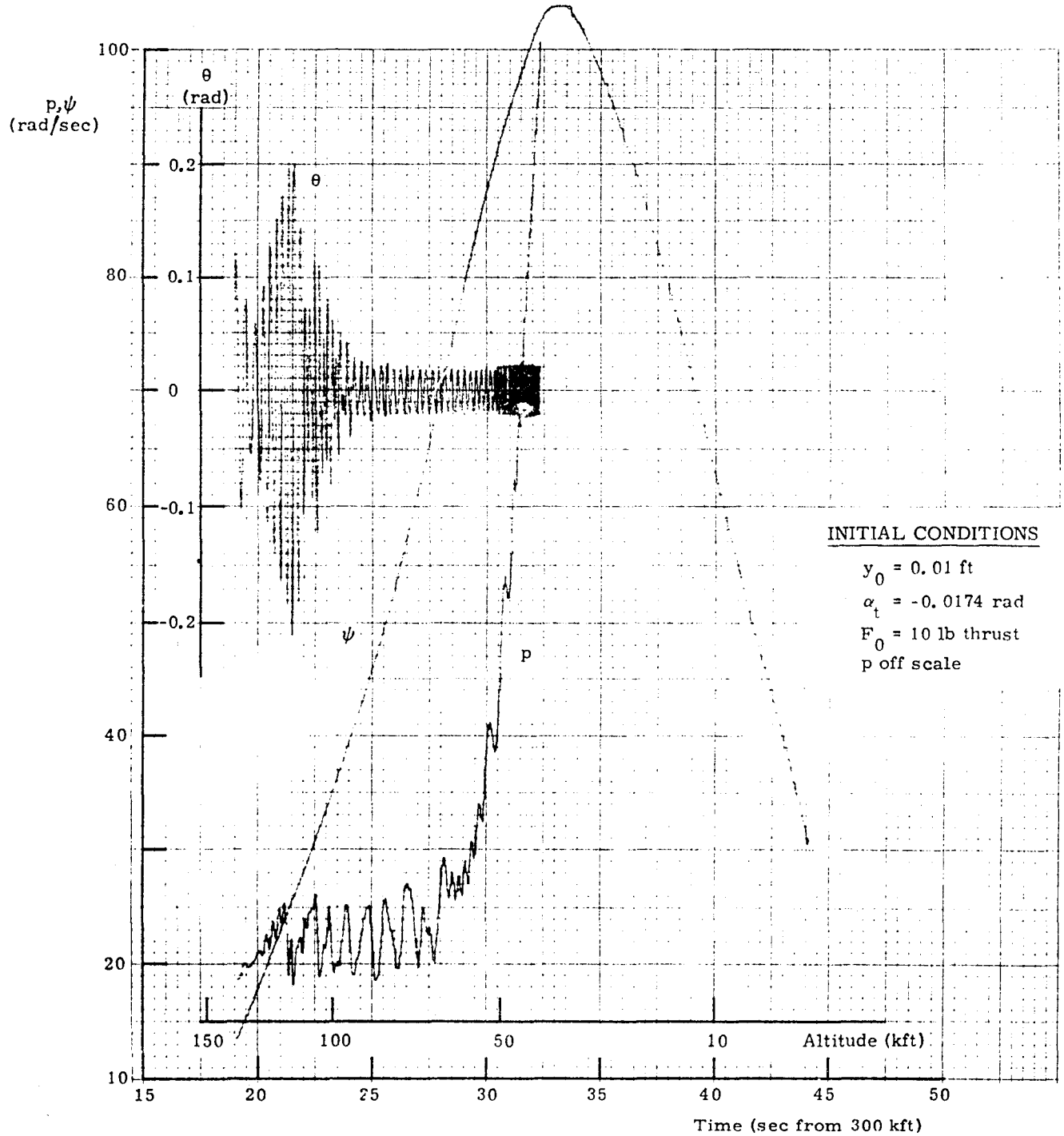

Figure 24. Analog Simulation with Roll Control (Large Asymmetries)

[redacted]

UNCLASSIFIED

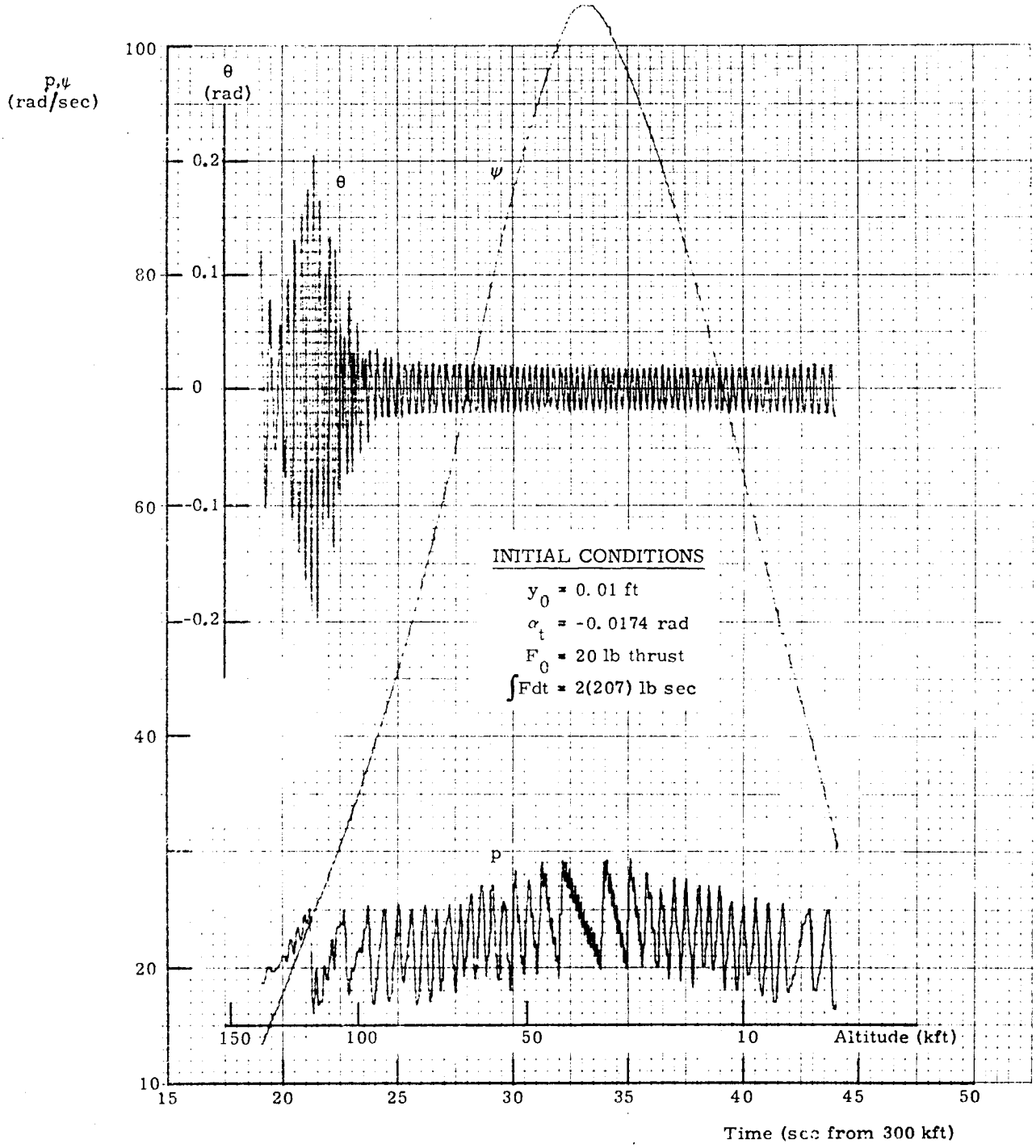

Figure 25. Analog Simulation with Roll Control (Large Asymmetries) Higher Control Thrust

UNCLASSIFIED

[redacted]

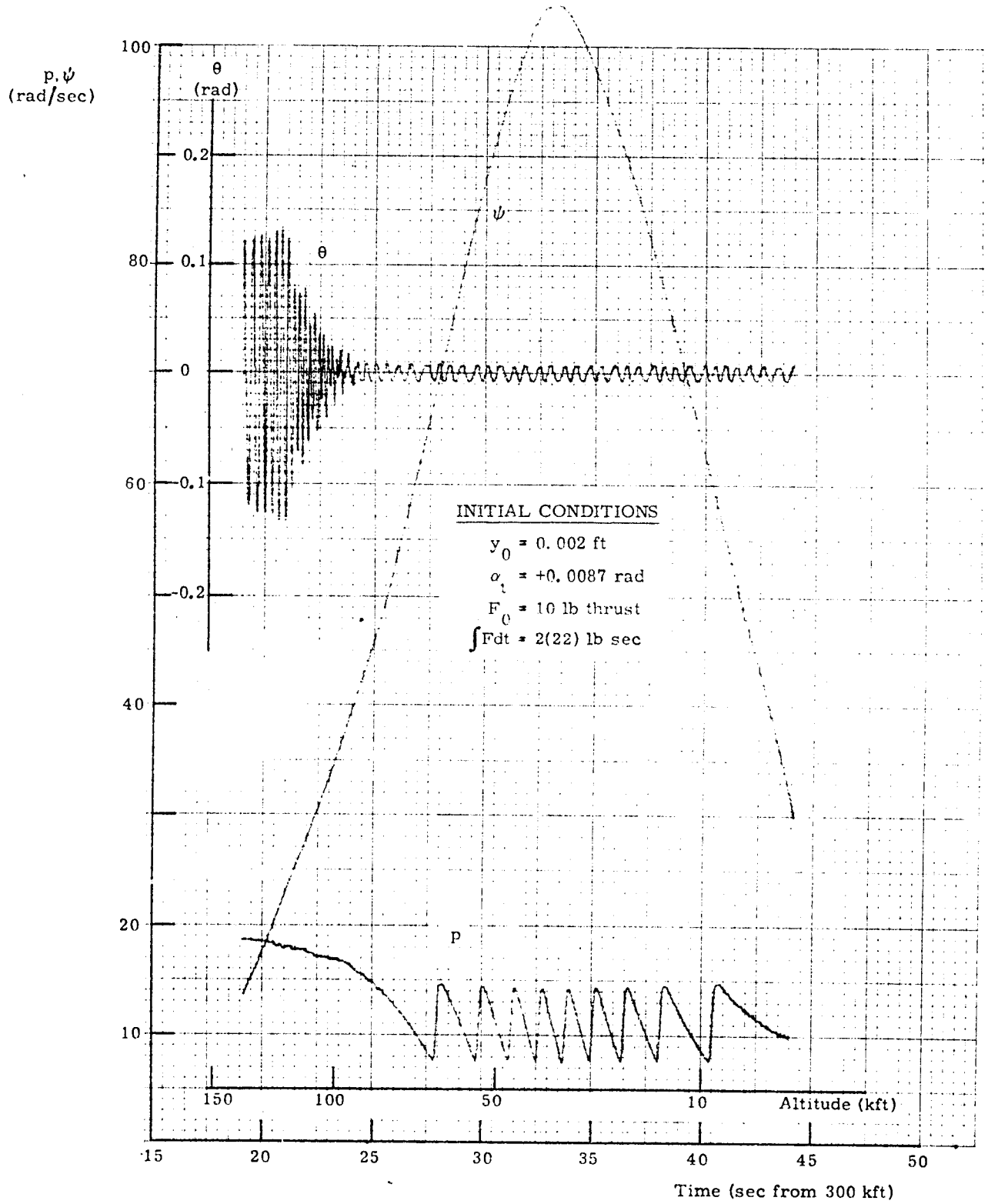

Figure 26. Analog Simulation with Roll Control (Small Asymmetries)

Equation 12 requires that $2r_mF_0 > 1.63$ lb ft; $2r_mF_0 = 10$ lb ft was used. Equation 23 requires that $I > 35$ lb sec; $\mathcal{J}_{SiM} = 44$ lb sec was obtained.

The roll rate attempted to decrease and roll through zero, but the control system prevented this and established the stable limit cycles analyzed in this report.

Figure 27

Assume

$$y_0 = 0.002 \text{ ft}$$

$$\alpha_t = -0.0087 \text{ rad.}$$

With the above values and 100 pounds thrust, the undesirable limit cycle analyzed previously in Example 8 resulted. The total impulse from this system was 720 lb sec when only 45 sec would have been sufficient.

Comparison Between Digital and Analog Computer Simulations

The analog computer simulations in this study utilize an extremely simplified aerodynamic model in order to achieve fast, inexpensive, and flexible simulation of a reentry vehicle with a roll control system.

In order to verify the accuracy of these simulations, comparisons with complete 6-degree-of-freedom (6DOF)[8] digital computer solutions will now be given.

Figure 28 compares the analog and 6DOF for the initial conditions $\alpha_t = 0.0087$ rad and $y_0 = 0.002$ ft (0.5 degree out of plane trim angle and 0.024-inch CG offset). From this figure, the analog appears to be an excellent approximation to the 6DOF for small values of α_t and y_0. A 1.0-second difference in time base appears in this comparison. This difference may be attributed to a 1-second error in the initializing of the dynamic pressure input function generator in the analog computer. It should be noted that the time required to obtain the analog simulation was 10 minutes, while the 6DOF solution required 28.01 minutes of IBM 7090 computer time.

A simple roll control model was added to the 6DOF program by incorporating a roll control torque into the differential equation for the roll rate. The switching of this control torque was accomplished by programming the switching function of

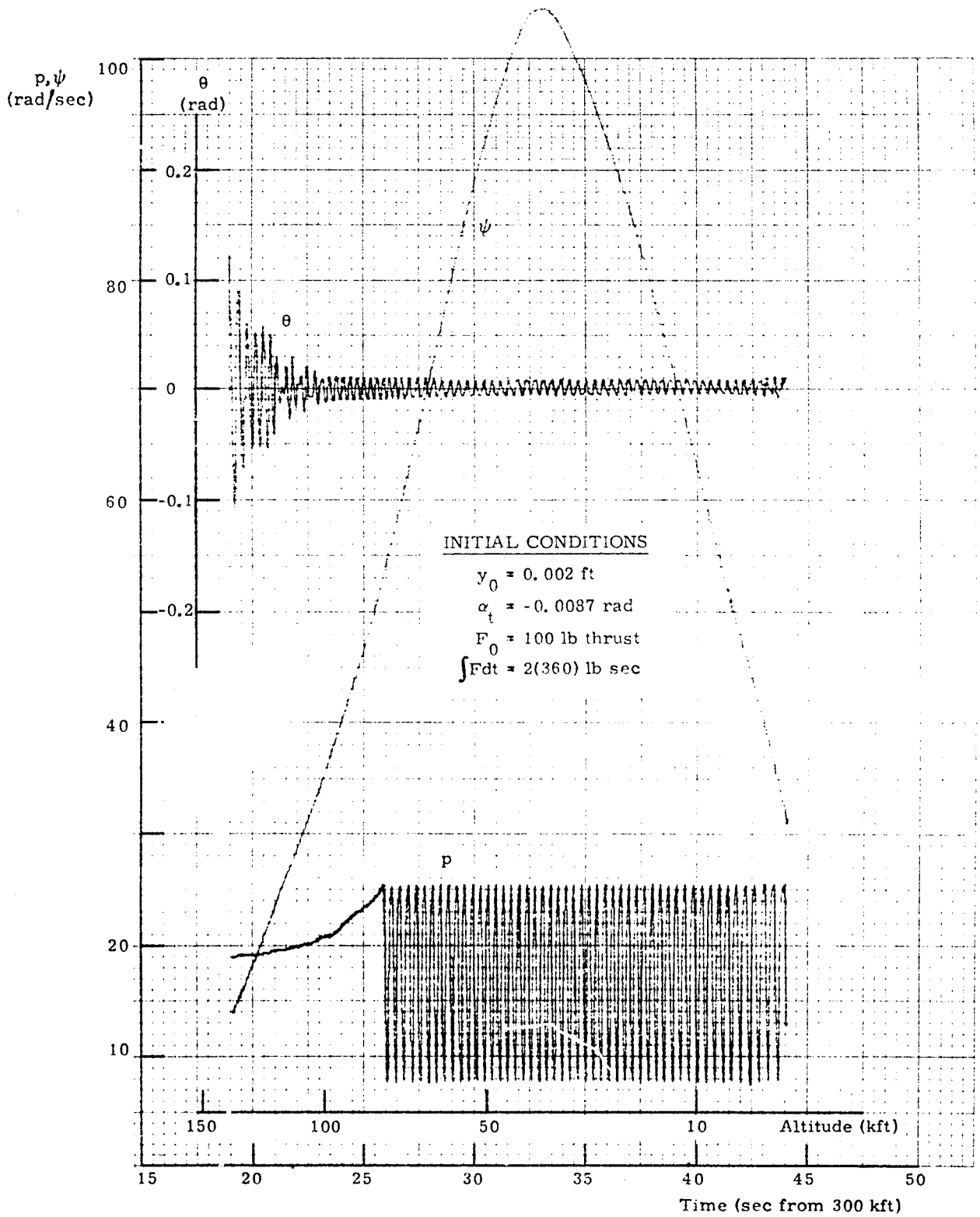

Figure 27. Analog Simulation with Roll Control (Undesirable Limit Cycle)

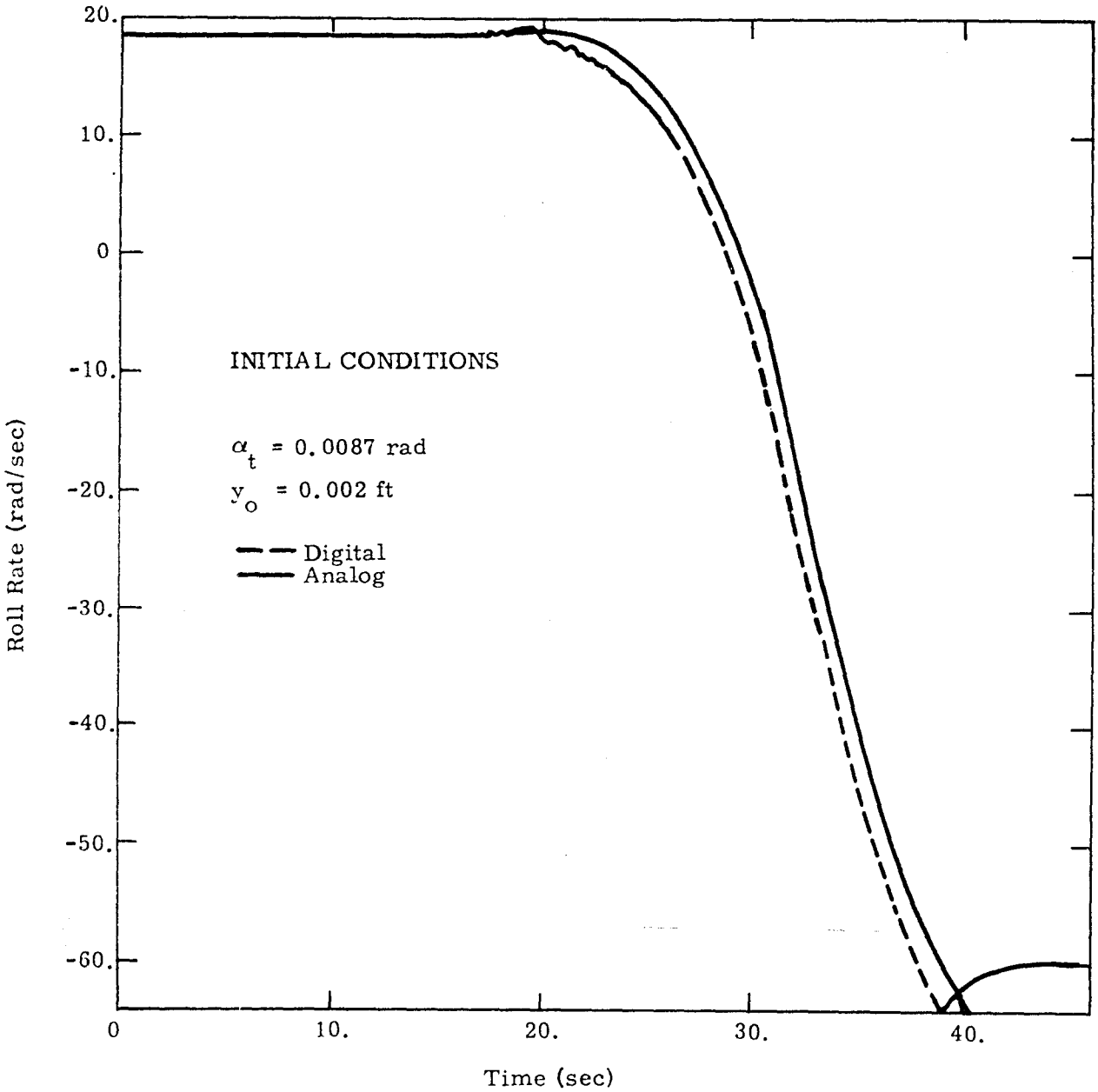

Figure 28. Comparison Between Digital and Analog Simulations

Figure 15b into the 6DOF code. The resulting roll behavior of the 6DOF simulation is given in Figure 29.

The initial conditions for this simulation were identical to those of the analog case given in Figure 22. The analog and digital solutions agree closely in both switching points and thruster turn-on and turn-off times.

The analog simulation required 10 minutes, while the 6DOF required 18.8 minutes. The reduction in 6DOF time is the result of the stabilizing effect of the roll control system on the integration routines in the 6DOF model. With stable integrations, longer solution time increments are possible, and hence shorter total running time results.

Desiderata

Because of the exploratory nature of this study, there are many unanswered questions concerning RV instability phenomena and techniques for control. It is therefore the intent of this section to identify areas within Sandia Laboratories where further investigation is desired and to briefly outline the scope required.

Stability Before and After X-Ray Exposure

Vehicle damage caused by X-ray effects will produce aerodynamic asymmetries which may produce substantial roll torques.

Therefore, greater control torque may be necessary to provide vehicle stability after an X-ray intercept. However, it has been shown in this report that control system instability may occur with large control torque and small vehicle asymmetries. Thus, paradoxically, a roll control system which could stabilize a damaged vehicle may result in an unstable system if the vehicle is undamaged.

It is therefore desirable to investigate the stability of the RV-control system both before and after X-ray intercept.

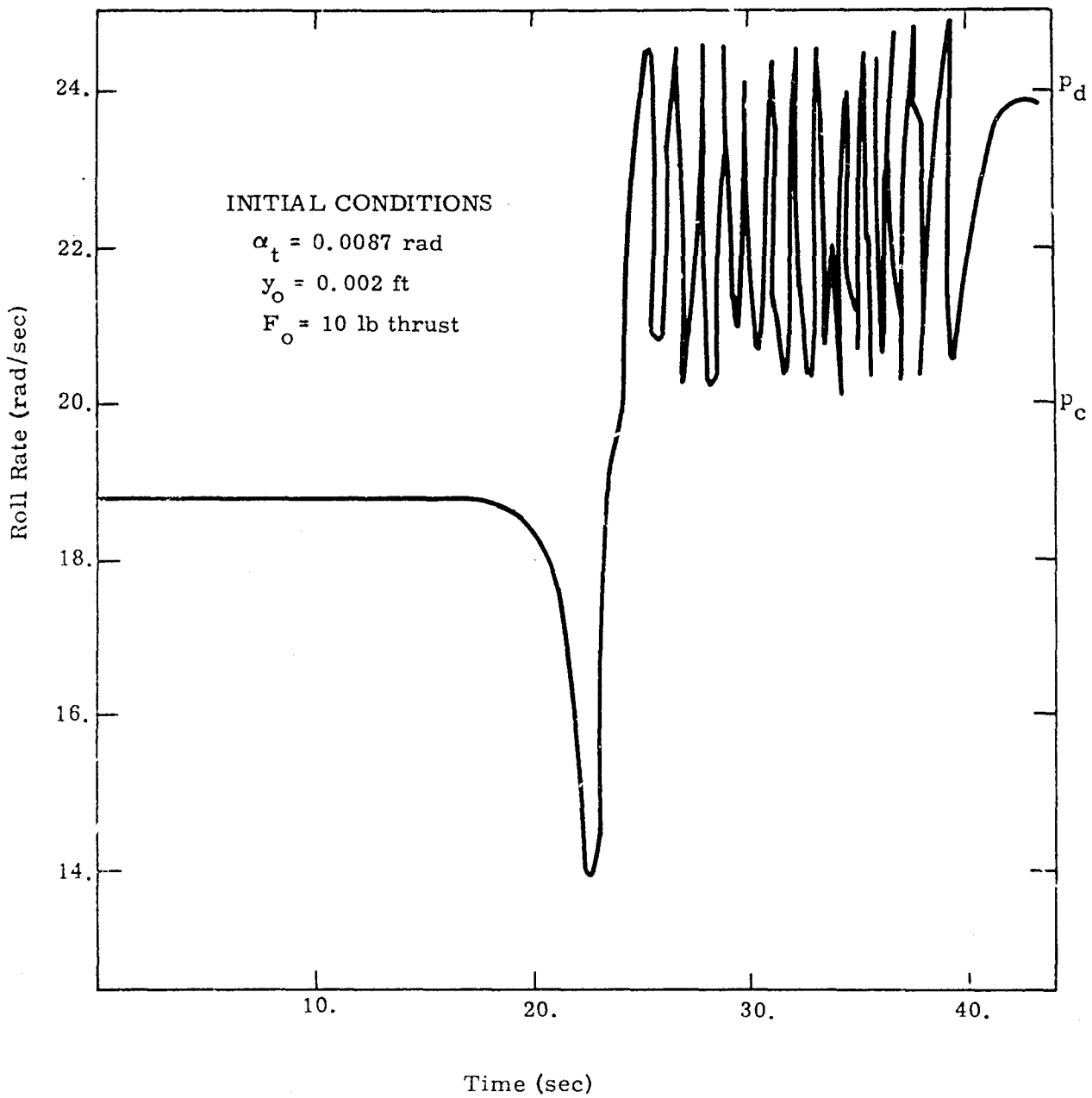

Figure 29. Digital Simulation with Roll Control

Magnitude of Aerodynamic Roll Torque

The magnitude of the aerodynamic roll torque during reentry must be known in order to design a roll control system with sufficient control thrust and fuel. For the case of peaceful reentry (i. e., no enemy interceptors), this problem is presently under investigation.[3] For the case of X-ray intercept preceding or coinciding with reentry, a study of induced roll torques is desired which will

1. Utilize the phenomenology analysis being developed in the Sandia Laboratories Materials and Process Department and the Exploratory Systems Department, to estimate the amount of material-blowoff induced center of gravity offset and to determine the thermal and impulse effects caused by X-ray fluence.

2. Employ the materials, structures, stress, and thermodynamic analyses developed in the Engineering Analysis Department to determine the aerodynamic shape and mechanics of the RV.

3. Utilize analytical and simulation techniques under development in the Aerothermodynamics Organization to determine the flight characteristics of the damaged RV.

This study should be parametric in outlook in order to facilitate the analysis of several different advanced reentry vehicles.

Effects of In-Plane Trim Angle

Since this report has been concerned with the roll instabilities caused by an out-of-plane trim angle, the in-plane trim has been ignored. It is therefore desirable to investigate the effects of an in-plane trim angle on vehicle stability and dispersion from target due to non-zero roll acceleration.

Techniques for converting vehicle asymmetries before and after X-ray exposure into in-plane and out-of-plane components are also desirable.

Sizing and Component Analysis for Roll Control

In order to determine the feasibility of an active roll control system, component realizability and/or existence must be established. An estimate, based on a fluidic control system with nonpropellant hydrazine thrusters, is 12 lbs weight, 250 cu. in. volume.

The estimated weight breakdown is:

Motors	0.75 lb ea x 4	=	3.0 lb
Fuel		=	2.5
Container		=	0.75
Fuel Valves	0.5 ea x 2	=	1.0
Fluidics		=	0.75
Power Supply		=	1.5
Start Valves	0.25 x 2	=	0.5
Plumbing		=	0.75
Support		=	1.25
	TOTAL		12.0 lb

Fluidic and thruster components development is presently underway in the Electromechanical Development Department. Together with knowledge of the control torques required, this development will provide the sizing analysis desired.

Investigation of other means for obtaining control torque is also desirable. Cold gas, hot gas, and hydrazine thrusters should be compared. The feasibility of obtaining aerodynamic roll control with split flaps should also be investigated. This would be an especially attractive scheme for maneuvering reentry vehicles, because the flaps may be moved in unison, with zero roll rate, to obtain transverse flight control. Roll control may then be an integral part of the maneuver control system.

Because electromechanical sensing, utilizing a rate gyro and electronic circuitry, offers a greater growth potential than fludics when additional system complexity and compatibility are required, studies in this area are desirable.

Tradeoff Study of Active and Passive Roll Control

Since the objective of the roll control system is to insure the roll stability of small RV's, the question arises as to the necessity of active control. That is, can the estimated 12 lb control system weight be allocated to additional structure or ballast for the RV in order to achieve stability? It is therefore desirable to explore the tradeoff between active and passive stability control as a function of RV configuration and X-ray induced damages.

Note that the Sandia concept of a removable X-ray shield is in the above sense also a type of semipassive stability control. When the RV receives X-ray fluence, the shield sustains the damage. In order to insure stability, the damaged shield is then discarded by a system which senses roll instability. The RV then reenters with clean aerodynamic characteristics.

Compensation and Adaptation Study

Since the magnitude and rate of change of the aerodynamic roll torque varies over a wide range during reentry, it is desirable to investigate the feasibility of control system compensation in order to minimize fuel requirements and maximize performance. The feasibility of providing an adaptive or compensatory feature to the control system should also be investigated for the case of an X-ray damaged vehicle.

Both linear and non-linear systems should be included in this study.

LIST OF REFERENCES

1. Fuess, B. F., "Impact Dispersion Due to Mass and Aerodynamic Asymmetries," AIAA Journal of Spacecraft, Vol. 5, No. 10, pp. 1402-1403, October 1967.

2. Vaughn, H. R., "The Effect of Thermal Distortion on Reentry Vehicle Roll-Rate Behavior," (U) SC-DR-68-418, RS 3410/1208, July 1968.

3. Vaughn, H. R., "Boundary Conditions for Persistent Roll Resonance on Re-Entry Vehicles," AIAA Journal, June 1968.

4. Vaughn, H. R., "Spin Up and Roll Reversal of Reentry Vehicles," SC-RR-68-219, May 1968.

5. Bennett, M. D., "Motion of a Small Reentry with Slight Configurational Asymmetries," SC-WD-66-499, October 1966.

6. Norris, G. R., Jr., "Theory and Practice of Measuring Mass Properties," SC-TM-67-2945, February 1968.

7. Solodownikow, W. W., "Grundlagen Der Selbsttätigen Regelung" Band II, R. Oldenbourg Verlag, München Vebverlag Technik, Berlin, 1959.

8. SRD, Internal Sandia Laboratories correspondence, A. F. Veneruso, 5635 to Distribution, Re: Necessary Conditions for Persistent Roll Resonance on Castor (U), dtd May 10, 1968, RS 5635/260.

DISTRIBUTION:

1/82A - Commanding General
U.S. Army Missile Command
Redstone Arsenal, Alabama 35809
Attn: AMSMI-KAAM

2/82A - University of California
Lawrence Radiation Laboratory
P.O. Box 808
Livermore, California 94550

3/82A - Aerospace Corporation
P.O. Box 1308
San Bernardino, California 92404
Attn: D. H. Platus

4/82A - Director, Air Force Weapons Laboratory
(WLIL/E. Lou Bowman)
Kirtland Air Force Base
New Mexico 87117

5/82A - Commander, Air Force Special Weapons Center
Kirtland Air Force Base, New Mexico 87117
Attn: Chief, Mail & Message Div.

6/82A - Los Alamos Scientific Laboratory
P.O. Box 1663
Los Alamos, New Mexico 87544
Attn: Report Librarian

7/82A - Office, Mr. William Carter
Asst. Director (Nuclear Programs)
Director of Defense Research and Engr.
Room 3E-1071, The Pentagon
Washington, D.C. 20301

8/82A - Advanced Research Projects Agency
Pentagon Room 3D-148
Washington 25, D.C.

9/82A - Kaman Nuclear
Division of Kaman Aircraft Corp.
Garden of the Gods Road
Colorado Springs, Colorado 80907
Attn: F. J. Barbera

10/82A - AVCO Corporation
Research and Advanced Development Div.
201 Lowell Street
Wilmington, Mass. 01887
Attn: Dr. H. Gold

DISTRIBUTION: (cont)

11/82A - Document Control Office
Office, Chief of Research and Develop.
Depart. of the Army
Room 3D-442, The Pentagon
Washington, D.C. 20310

12/82A - U.S. Atomic Energy Commission
Division of Technical Information,
Reports Section
Headquarters Library, G-017
Washington, D.C. 20345

13/82A - U.S. Atomic Energy Commission
Albuquerque Operations Office
P.O. Box 5400
Albuquerque, New Mexico 87115

14/82A - U.S. Atomic Energy Commission
Sandia Area Office
P.O. Box 5400
Albuquerque, New Mexico 87115

15/82A - Headquarters, Field Command
Defense Atomic Support Agency
Sandia Base
Albuquerque, New Mexico 87115

16/82A - Director, Special Projects
Department of the Navy
Washington, D.C. 20360

17/82A - SAMSO (SMYSA/Capt. M. Halbert
Norton Air Force Base,
California 92409

18/82A - Chief, Administrative Services Br.
Defense Atomic Support Agency
Washington, D.C. 20305

19/82A - Commanding Officer
Picatinny Arsenal
Dover, New Jersey 07801
Attn: Restricted Data Control Officer

20/82A - Commanding General
White Sands Missile Range
White Sands, New Mexico 88002
Attn: STEWS-AD-M

21/82A - Chief, SENSCOM
Bell Telephone Laboratories, Inc.
Whippany, New Jersey 07981

DISTRIBUTION: (cont)

22/82A - D. B. Shuster, 1200
23/82A - W. C. Myre, 1210
24/82A - R. C. Beckmann, 1212
25/82A - O. M. Stuetzer, 1220
26/82A - C. R. Blaine, 1221
27/82A - H. M. Stoller, 1222
28-29/82A - R. H. Braasch, 1223
30/82A - A. J. Chabai, 1224
31/82A - W. A. Gardner, 1500
32/82A - D. M. Olson, 1510
33/82A - B. E. Arthur, Jr., 1520
34/82A - T. B. Lane, 1540
35/82A - R. M. Tidwell, 1546
36/82A - C. H. Mauney, 1548
37/82A - S. D. Spray, 1652
38/82A - T. M. Burford, 1700
39/82A - J. W. Weihe, 1710
40/82A - R. G. Clem, 1730
41/82A - W. F. Roherty, 1731
42/82A - G. W. Hauer, 1732
43/82A - R. L. Peurifoy, 1820
44/82A - D. R. Cotter, 1830
45/82A - L. D. Smith, 2300
46/82A - E. N. Leslie, 2322
47/82A - R. E. Fox, 2325
48/82A - J. D. Cyrus, 2325
49/82A - L. Gutierrez, 8100
50/82A - D. E. Gregson, 8130
51/82A - J. F. Barham, Jr., 8131
52/82A - J. E. Marion, 8133
53/82A - A. Y. Pope, 9300
54/82A - R. C. Maydew, 9320
55-56/82A - H. R. Vaughn, 9325
57/82A - D. F. McVey, 9328
58/82A - K. J. Touryan, 9340
59/82A - J. K. Cole, 9341
60/82A - J. L. Tischauser, 9420
61/82A - A. R. Iacoletti, 9422
62/82A - W. F. Carstens, 3410, Attn: R. S. Gillespie, 3411
63/82A - B. R. Allen, 3421
64/82A - B. F. Hefley, 8232
65-82/82A - C. H. Sproul, 3428-2

hlsp

[redacted]

[redacted] in whole or in part, without [redacted]